

ON THE SIMULATION AND OPTIMAL DESIGN OF
HYDRO-MECHANICAL DRIVES FOR MITRE GATES IN
NAVIGATION LOCKS

Aleksander Proszanski

A THESIS
in the
FACULTY OF ENGINEERING

Presented in partial fulfillment of the
requirement for the Degree of
Master of Engineering at
Concordia University
Montréal, Québec, Canada

September, 1976

ABSTRACT

ALEKSANDER PROSZANSKI

ON THE SIMULATION AND OPTIMAL DESIGN OF HYDRO-MECHANICAL DRIVES FOR MITRE GATES IN NAVIGATION LOCKS

A description is given of lock gates and the types of loads acting on gate drives. The technique of Power Bond Graphs is adopted to simulate a hydro-mechanical drive of a mitre gate. The mathematical model developed is used to carry out an optimization to minimize the power requirement and operating costs of the drive. Also, the model is used to estimate the effect of water surges on the operating times of the gates.

Tests were carried out on a prototype hydro-mechanical gate drive installed on the St. Lawrence Seaway and results presented. The results from the prototype tests are compared with those predicted by the mathematical model and found to correlate well.

It is found that water resistance is the preponderant load on a mitre gate drive. To overcome the gate loads, the most efficient drive mechanism is shown to be hydro-mechanical employing a single constant power pump in its hydraulic circuit; the pump adjusts its output pressure to suit the all important water resistance. It was also found that the most economical power of mitre gate drives for the St. Lawrence Seaway is 25 HP.

ACKNOWLEDGEMENTS

The author wishes to thank his Supervisor, Dr. S. Sankar for his valuable advice and the wholehearted help given during the preparation of this dissertation.

The author also wishes to thank the Concordia University Fluid Control Centre for making possible the extensive tests on the prototype installation.

Thanks are also due to the author's family for their uncomplaining patience during the preparation of this dissertation and to Mme R. Molleur who suffered the author's handwriting while typing this work.

TABLE OF CONTENTS

ABSTRACT	1
ACKNOWLEDGEMENTS	ii
LIST OF TABLES	vi
LIST OF FIGURES	vii
NOMENCLATURE	ix
 I INTRODUCTION	
1.1 General	1
1.2 Historical background	1
1.3 Modification to installed electro-mechanical gate drive.	4
1.4 Scope of dissertation	8
 II NAVIGATION LOCK GATES AND THEIR DRIVES	10
2.1 Introduction.	10
2.2 Drive mechanism for gates	15
2.3 General criteria for gate drive mechanisms.	16
2.3.1 Capital and operating costs.	16
2.3.2 Geometrical and space considerations	17
2.3.3 Compatibility with other lock machinery	17
2.3.4 Overload protection.	18
2.3.5 Gate locking	18
2.3.6 Power requirement.	18
2.3.7 Loads on Gate Machinery.	19
2.4 Hydro-mechanical gate drive mechanism	19
 III SIMULATION OF HYDRO-MECHANICAL MITRE GATE DRIVES	22
3.1 Preamble.	22
3.2 General	24
3.3 Loads on mitre gate drive mechanism	24
3.3.1 Frictional load.	24
3.3.2 Wind load.	25
3.3.3 Water surging in lock.	25
3.3.4 Effect of inertia load on gate	26
3.3.5 Water resistances.	26
3.3.6 Other loads.	27

3.4	Assumptions	28
3.5	Mathematical modeling of mitre gate drives. .	30
3.5.1	The governing equations.	32
3.7	Digital computer simulation	43
IV	PERFORMANCE CHARACTERISTICS OF PROTOTYPE HYDRO-MECHANICAL GATE DRIVE ON THE ST. LAWRENCE SEAWAY	45
4.1	General	45
4.2	Design constraints imposed on hydro-mechanical drive mechanism.	45
4.3	Functional description of the hydraulic circuit	52
4.4	Performance tests of hydro-mechanical gate drive	57
4.4.1	General.	57
4.4.2	Measurement procedure and recording. .	58
4.4.3	Test results	59
4.4.4	Corrections to pump delivery	65
4.4.5	Hydraulic power developed in the pumps	67
4.4.6	Conclusion	68
4.5	Correlation of mathematical model with prototype test results	69
4.5.1	Hydraulic system pressure.	70
4.5.2	Gate operating time.	72
4.5.3	Hydraulic motor speed.	72
4.5.4	Other variables.	74
V	OPTIMIZATION	77
5.1	General	77
5.2	Assumptions	77
5.3	Utilization costs	78
5.4	Cost of gate drive modification	80
5.5	Optimum power	80
5.6	Effect of water surging	83
VI	CONCLUSIONS	84
6.1	General	84
6.2	Discussion of mathematical model and prototype results	84
6.3	Applications.	86
6.4	Future work	87

APPENDIX A	
Power bond graphs	88
APPENDIX B	
Computer program listings	103
APPENDIX C	
Additional tests of prototype drive	117
APPENDIX D	
Proposed control circuit for hydro-mechanical gate drives	126

LIST OF TABLES

TABLE	DESCRIPTION	PAGE
3.1	Values of parameter P_t	42
4.1	Lock gate operation pattern	60
4.2	Hydraulic motor speed comparison.	73
4.3	Simulated performance variables for gate opening, 50 HP drive.	75
4.4	Simulated performance variables for gate closing, 50 HP drive.	76
5.1	Gate operating times.	79
5.2	Effect of water surging	82
A1	Basic terms and symbols for power bond graphs	90
C1	Synopsis of test runs	121

LIST OF FIGURES

FIGURE	DESCRIPTION	PAGE
1.1	The St. Lawrence Seaway	2
1.2	Electro-mechanical gate drive mechanism . .	3
1.3(a)	Hydraulic circuit for mitre gate drive mechanism	6
1.3(b)	Component list for hydraulic circuit for mitre gate drive	7
2.1	Sliding gate	11
2.2	Vertical lift gate	12
2.3	Sector gate	12
2.4	Mitre gate	14
2.5	Hydro-mechanical gate drive	20
3.1(a)	Schematic representation of simulated drive	23
3.1(b)	Simulated circuit	31
3.2	Power bond graph	33
3.3	Gate operating drive	37
3.4	Model gate test torques VS pivoting angle θ	41
4.1	Torque characteristics of an electro-mechanical gate drive	48
4.2	Hydraulic system flow vs system pressure . .	49
4.3	Sector gate pinion speed vs time	50
4.4	Hydraulic motor torques vs time	53
4.5(a)	Time vs hydraulic motor speed-gate closing	54
4.5(b)	Time vs hydraulic motor speed-gate opening	55
4.6	Actual traces	61
4.7	Gate opening characteristics	62
4.8	Gate closing characteristics	63

FIGURE	DESCRIPTION	PAGE
4.9	Pressure traces from prototype and model	71
5.1	Cost optimization	81
A2	1-junctions	93
A3	Simple hydraulic systems.	100
C1	Some measured electrical power curves . .	118
C2	Gate opening characteristics.	122
C3	Gate closing characteristics.	123
D1	Schematic of control circuit.	127
D2	System circuit.	130

NOMENCLATURE

		UNITS
a	amplitude of static head	m
A	submerged area	m^2
A_p	equivalent piston area	m^2
A	angle	rad
B	angle	rad
b	constant	s
HP_p	power to pump	W
I_j	inertia effect	W
K_1	pump leakage constant	m^3/s
K_2	motor leakage constant	m^3/s
K_3	constant	-
K_4	constant	-
MA	mechanical advantage	-
N_d	motor to gate drive efficiency	-
$N_{mech.}$	mechanical efficiency of motor	-
$N_{p_{mech.}}$	mechanical efficiency of pump	-
N_s	ships annually	1/year
P_a	system pressure	Pa
P_i	pump pressure before losses	Pa
P_f	pressure loss across pump	Pa
P_h	hydrostatic pressure	Pa
P_t	parameter	$K_g \cdot m^2/rad^2$
Q_a	flow to motor	m^3/s
Q	pump flow before losses	m^3/s
Q_l	leakage flow	m^3/s

		x
		UNITS
Q_r	relief flow	m^3/s
R	gate radius	m
R_f^g	gate frictional loss	W
R_f^p	pump frictional loss	W
R_f^m	motor frictional loss	W
R_g	gate water resistance	W
R_l	motor and pump leakage loss	W
R_p	equivalent piston radius	m
R_r	relief loss	W
R_s	surge effect	W
t	time from start of surge	s
T_{now}	time from start of gate operation	s
T_a	motor output torque	N-m
T_g	gate input torque	N-m
T_f^g	gate friction torque	N-m
T_j^g	gate inertia torque	N-m
T_{now}^h	gate operation time, hydro-mech. drive	s
T_m	motor input torque	N-m
T_f^m	motor friction torque	N-m
T_s	time saving	s
V_m	motor constant	m^3/rad
V_s	apparent pump flow	m^3/s

UNITS

$\$w^t$	utilization benefit	\$
$\$w$	utilization benefit per sec.	\$ /s
$\$pr$	present value savings	\$
P_r	pressure across relief valve	Pa
T_{now}	change in gate operating time	s
T_{now}^e	time change, hydro-mech. drive	s
T_{now}^h	time change, electro-mech. drive	s
T_g^e	gate torque change, electro-mech. drive	N-m
T_g^h	gate torque change, hydro-mech. drive	N-m
$\Delta\omega_g^e$	gate speed change, electro-mech. drive	rad/s
$\Delta\omega_g^h$	gate speed change, hydro-mech. drive	rad/s
$\Delta\omega_m^e$	equivalent motor speed change, electro-mech. drive	rad/s
$\Delta\omega_m^h$	equivalent motor speed change, hydro-mech. drive	rad/s
ω_g	gate speed	rad/s
ω_m	motor speed	rad/s
φ	angle	rad
θ	angle	rad
ρ	force density of water	N/m ³

CHAPTER I

INTRODUCTION

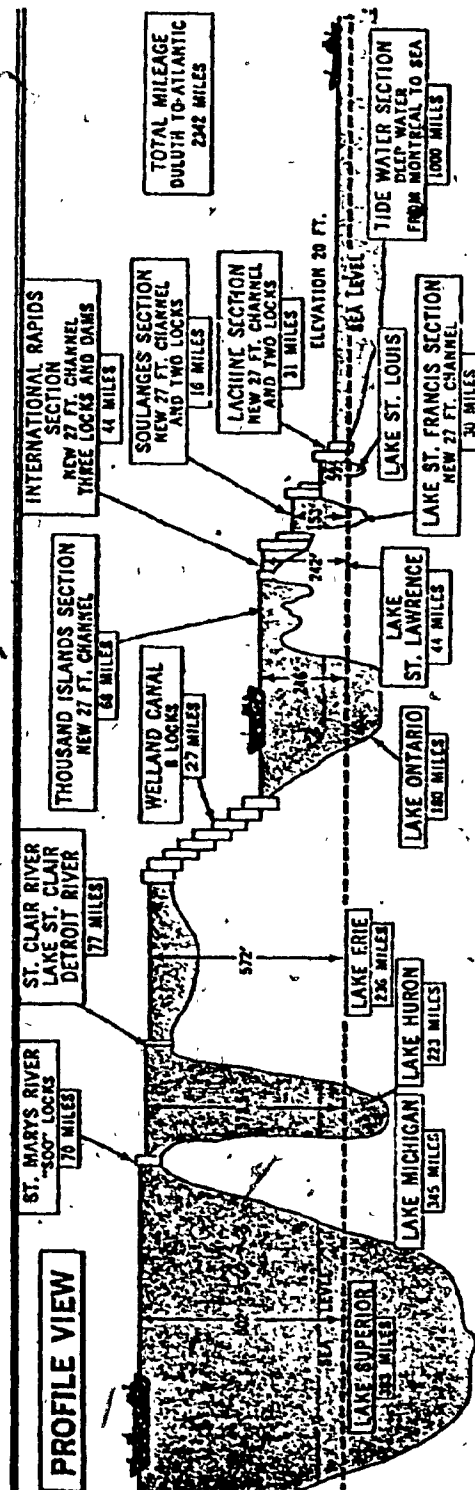
1.1 General

The St. Lawrence Seaway stretches from the lower reaches of the St. Lawrence River to the Lakehead at Lake Superior. A total of 15 locks are used to raise the vessels travelling the Seaway from sea level to the level of Lake Superior. A profile view describing the waterway and the procedures used in passing a vessel through a lock are shown in Figure 1.1; Lock gates of the mitre type are used throughout to achieve the desired differences in water elevations within the locks.

The mechanisms used to drive the lock gates in the St. Lawrence River section of the Seaway were put into operation in 1957. The modification of these mechanisms to obtain an optimal design from the point of view of operating cost will form the subject matter of this dissertation.

1.2 Historical Background

The above mentioned gate drive mechanisms were built to a design which is a variation of that used on the Panama Canal [2]. The operation of the electro-mechanical gate drive mechanism used on the Panama Canal is schematically shown in Figure 1.2.

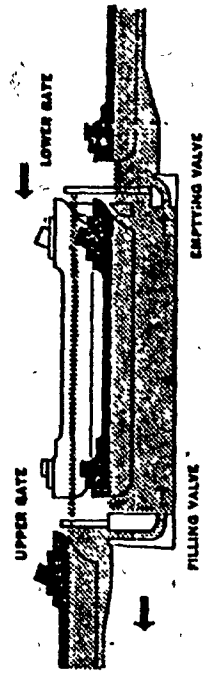


MAXIMUM SIZE OF SHIP PERMITTED TO TRANSIT THE SEAWAY:

Vessels not exceeding 730 feet overall and 76 feet extreme breadth may transit the Seaway. Vessels' masts must not extend more than 117 feet above water level.

locking procedures

All locks on the St. Lawrence Seaway are filled or emptied by gravity. To raise a vessel, for example, the upstream valves are opened and the water simply flows into the chamber through openings at the bottom of the walls. The following diagram illustrates the procedure:



The diagram portrays the following steps:

- 1: From the lower level the ship sails through the open gates into the lock and is secured to bollards near the side of the walls. The gates are closed.
- 2: The valves are opened and water is allowed to flow in, lifting the ship.
- 3: When the vessel reaches the higher level the upper gates are opened and the ship sails out.

To lower a vessel the above steps are reversed. It takes less than ten minutes to raise or lower the water level with more than 20 million gallons used for each lockage. Additional time, however, is required for the vessel to carefully manoeuvre in and out of the chambers. The average lockage requires approximately 33 minutes from the time the bow passes the approach wall until the stern is cleared of the outermost boom.

Figure 1.1 The St. Lawrence Seaway [1]

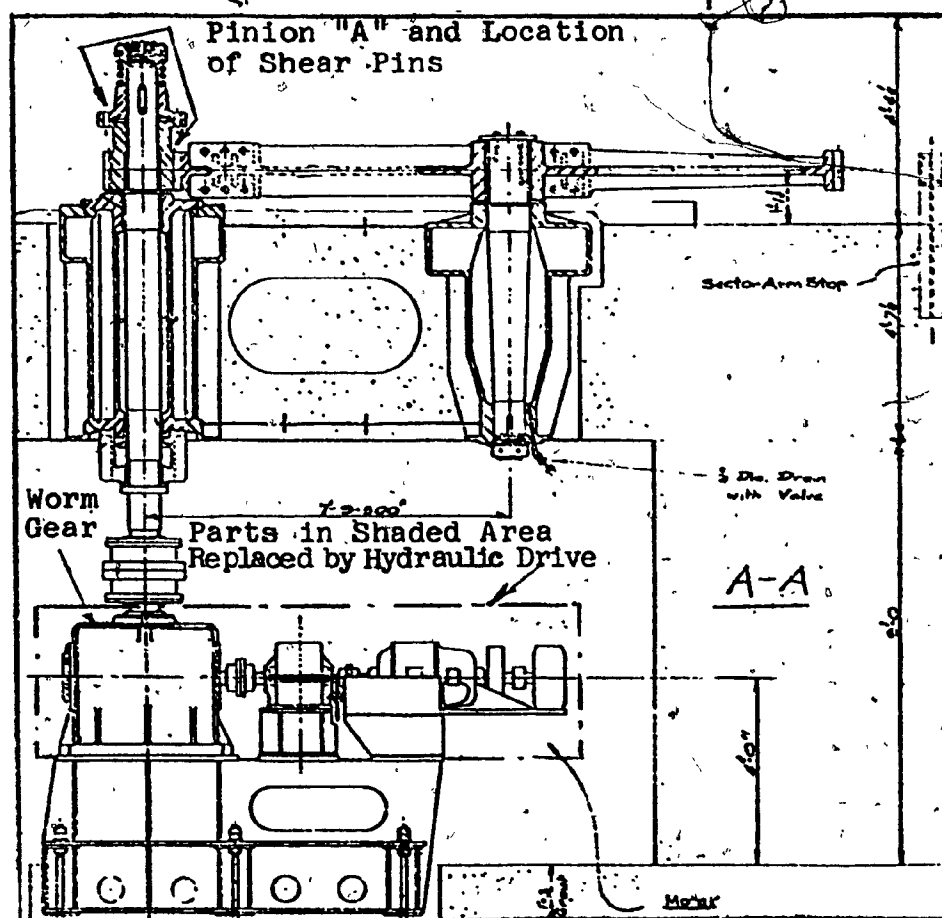
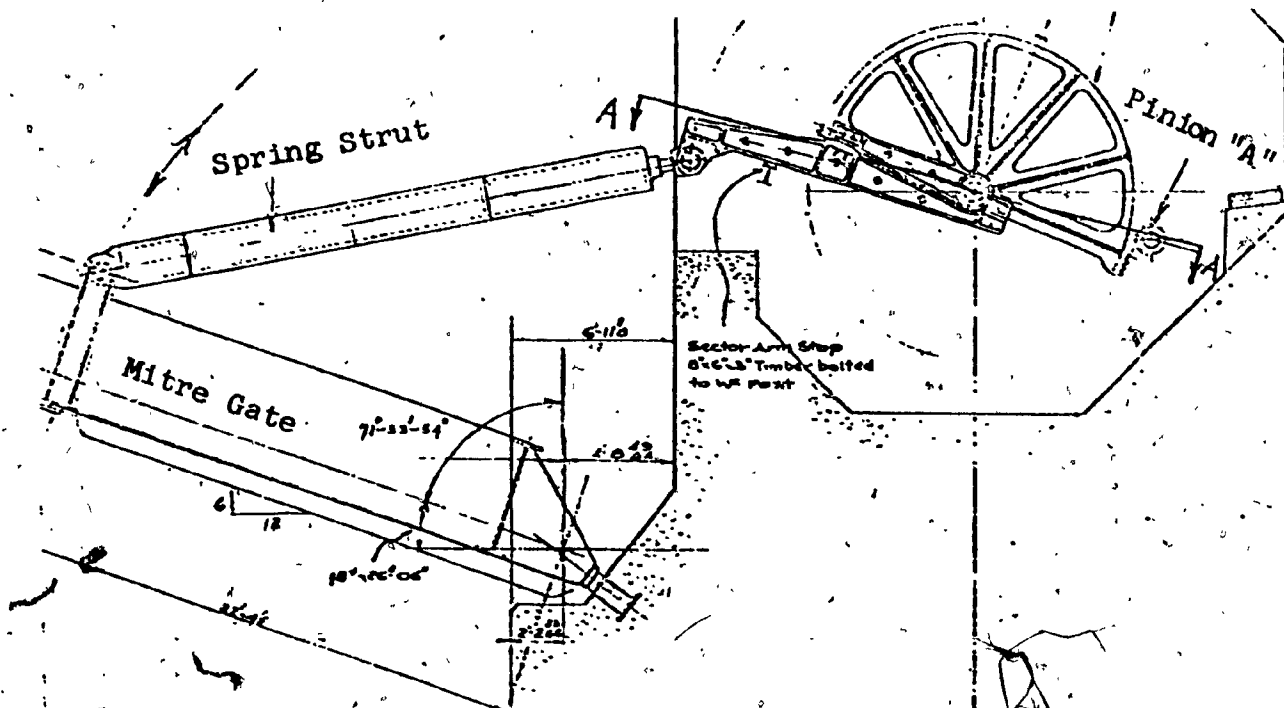


Figure 1.2 Electro-Mechanical Gate Drive Mechanism

The operation of this gate mechanism is described as follows. The gates are pivoted on their hinges to form a water dam to allow clear passage of a vessel. The motive force is provided by an electric motor driving a horizontal sector gear through a system of reduction gears including a worm gear which cannot be back-driven, i.e. the worm gear is self-locking. A shear pin arrangement is provided at the sector gear pinion to protect the worm gear from damage in case of an overload from the gate side of the mechanism. The original machinery performed well but for the following: The shear pin overload device built into the machinery became a source of high maintenance costs and delays to navigation, particularly at the time when ice was present in the Seaway. Also, it was thought the time to operate the gates could be reduced with savings to shippers and an increase in traffic capacity of the Seaway.

1.3 Modification to Installed Electro-Mechanical Gate Drive

A study was conducted with a view of overcoming the shear pin replacement problem and to speed up the operation of the gates. It was found that it would be feasible and economical to make the gate drive slip under any overload applied from the gate side and to cut the gate operating time if a hydro-mechanical drive mechanism is utilized.

The prototype of a hydro-mechanical gate drive machinery was built in 1974 and performance tested in 1975. The nature of the modification required is shown in Figure 1.2. The worm gear, largely responsible for the excessive number of shear pin breakages due to its self-locking, non-reversing feature, has been replaced by an hydraulic motor driven by a power-pack located nearby. A band brake has been provided around the hydraulic motor to enable locking the drive in any position without danger of "creep" under load due to leakage past hydraulic components. Power of the machinery has been increased from 20 HP to 50 HP in order to reduce the operating time of the gates. The hydraulic circuit for the modified machinery is shown in Figure 1.3.

To start the motion of the gates, pump No. 10 commences delivery while the output of pump No. 13 is by-passed through the piloted relief valve No. 19. The direction of gate movement is determined by valve No. 24. A pressure reduction is required for part of the operating time to relieve machinery stresses and this is provided for by allowing flow to the low pressure relief valve No. 21. To provide a breaking action on the gates in case they are driven by a surge of the water in which they are immersed, one of the counterbalance valves No. 27 or No. 28 is closed by vacuum in the hydraulic line supplying the motor.

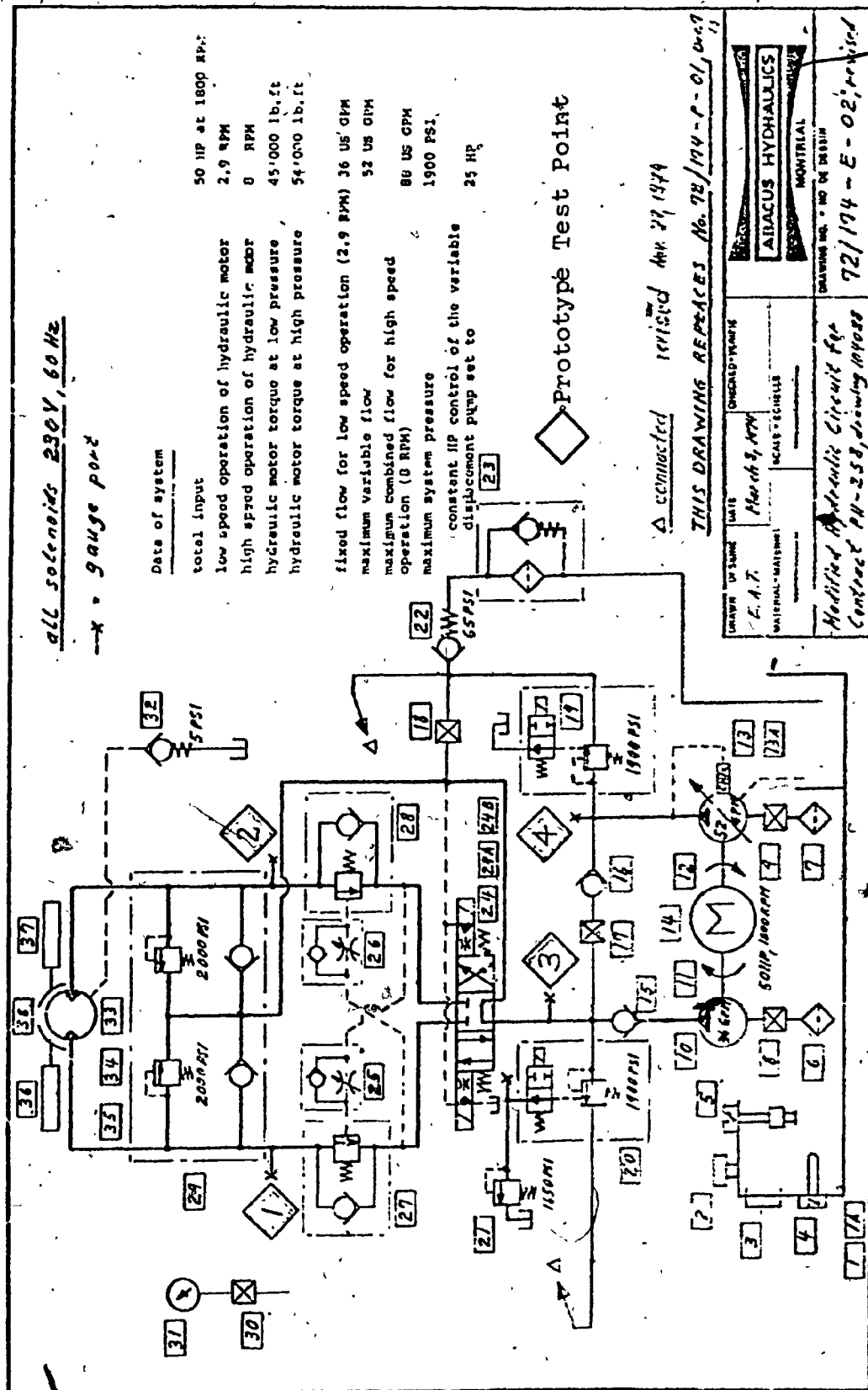


Figure 1.3(a) Hydraulic Circuit for Mitre Gate Drive

ITEM	DESCRIPTION	ITEM	DESCRIPTION
1	base frame	25	flow check valve
1A	reservoir	26	flow check valve
2	filler breather	27	counterbalance valve
3	view level gauge	28	counterbalance valve
4	temperature switch	29	dual relief- and make-up valve
5	level switch	30	needle valve
6	suction strainer	31	pressure valve
7	suction strainer	32	back pressure check valve
8	gate valve	33	hydraulic motor
9	gate valve	34	motor support bracket
10	vane pump	35	band brakes
11	flexible coupling	36	linear actuator
12	flexible coupling	37	linear actuator
13	piston pump	38	limit switches
13A	mounting bracket (pump)	39	swivel rod end clevis
14	electric motor	40	lever assembly
15	check valve	41	Flexmaster joint
16	check valve	42	Flexmaster joint
17	ball valve		
18	ball valve		
19	relief valve		
20	relief valve		
21	relief valve		
22	back pressure check valve		
23	micronic filter		
24	directional control valve		
24A	choke valve		
24B	valve base plate		

Figure 1.3(b) Component List for Hydraulic Circuit
for Mitre Gate Drive

The hydraulic motor will then be required to dissipate energy through one of the relief valves set at 2000 p.s.i. (14×10^6 Pa) depending on the direction of movement of the gate. Dissipating the energy prevents the gates from being slammed against their end position stops and being damaged. The constant power pump No. 13 supplies the motor only during the time of high speed operation, i.e. not during initial acceleration or final deceleration of the gates. The constant power feature of one of the pumps ensures that, over the operating range, maximum use is made of the machinery's power to minimize the gate operating cycle time. The product of pressure and flow is maintained constant so that an increase in torque load on the mitre gate produces a slowdown of the machinery and a rise in hydraulic pressure to overcome the load, whereas, a reduction of the gate load allows the machinery to move the gate faster by delivering large amounts of low pressure hydraulic fluid.

1.4 Scope of Dissertation

The initial part of this dissertation will describe various types of navigation lock gates, their drive mechanisms, their operating characteristics and the type of loads acting on the drives. The major advantages and disadvantages of the lock gates and their drives will also be discussed.

A mathematical model will be developed to simulate the performance of hydro-mechanical drive mechanisms for the most

complex drive such as a mitre gate. The validity of the model will be tested against the performance of a prototype hydro-mechanical drive installed and tested on the St. Lawrence River Section of the St. Lawrence Seaway in 1975. The model will be used to establish the relative importance of various parameters affecting the drive performance.

An optimization will be carried out to minimize the power requirement and the operating cost of the hydro-mechanical drive by establishing the size of the drive and its power pack.

The mathematical model developed will also be used to establish the maximum range of deviation from normal gate operating times due to water surges created in the waterway by passing vessels or operation of navigation lock equipment.

A short discussion will be provided of a proposed control system for the hydro-mechanical gate drive which will ensure safe deceleration rates for lock gates, without increasing the normal operating time of the gates.

Conclusions will be drawn based on the test results obtained from the prototype hydro-mechanical gate drive and from the simulation results via mathematical modelling.

CHAPTER II

NAVIGATION LOCK GATES AND THEIR DRIVES

2.1 Introduction

In this chapter the navigation lock gate configurations currently in use will be described. Also described will be gate drive machines and their essential characteristics, with particular emphasis on hydro-mechanical drives.

The descriptions are intended as background to the following formulation of the mathematical model of a hydro-mechanical gate drive mechanism described in the following chapter.

2.2 Types of Navigation Lock Gates

There are several types of navigation lock gates in use depending on water head and favoured areas of application:

The sliding gate, Figure 2.1, is usually used in tidal locks where water heads are low and sealing is not a major problem [3]. The gate runs on rollers and the projected wave creating area is small. The water resistance on the gate is small compared to the frictional force or the inertia effect of its mass and hence the gate drive loads are preponderantly inertial and frictional and usually quite predictable. The gate structure is uneconomical for high heads since hydrostatic forces create a large bending moment over the full span of the lock. Problems with supporting rollers are also frequent.

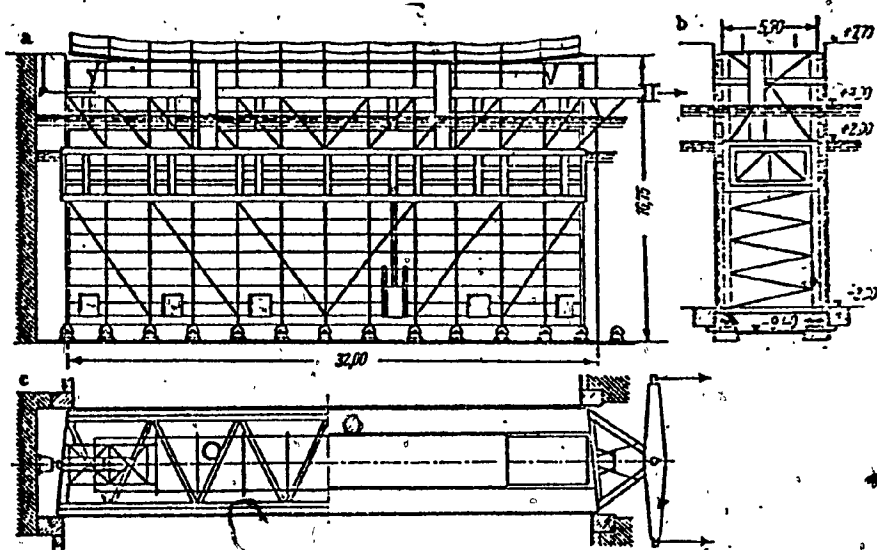


Figure 2.1 Sliding Gate [3]

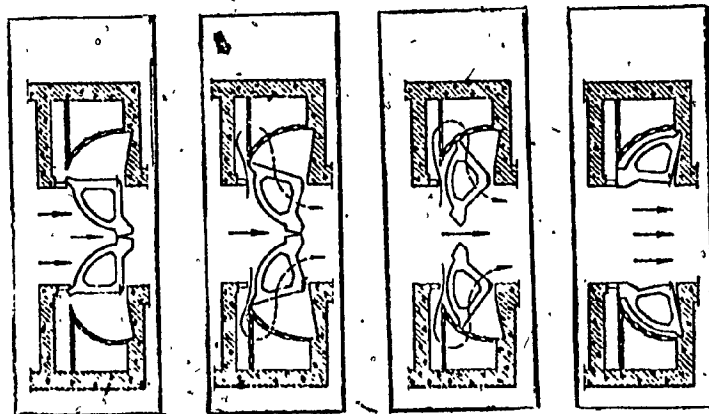


Figure 2.3 Sector Gate [3]

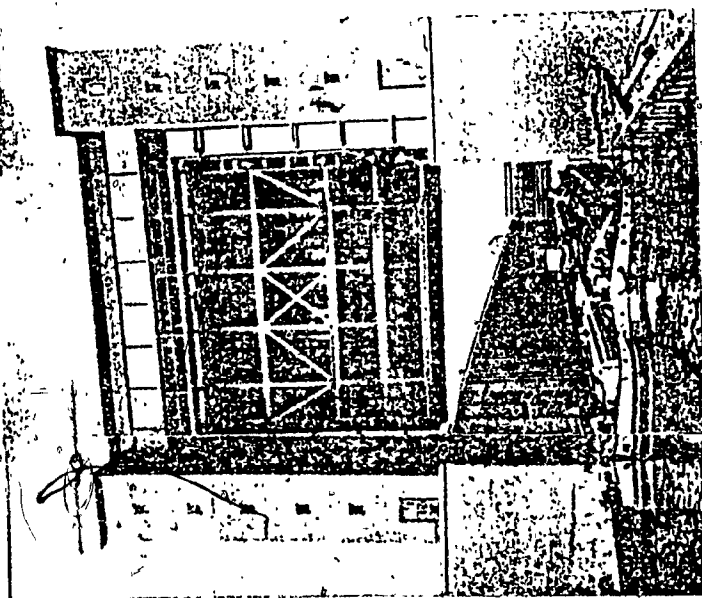


Figure 2.2 Vertical Lift Gate [3]

Vertical lift gate, Figure 2.2, is popular for "low profile" traffic canals used mainly by flat barges. It is not an ideal configuration for ocean vessels or for operating in freezing weather [3].

The sector gate, Figure 2.3, is an excellent safety gate in that it can be closed against a fully developed flow in a canal. This is because all hydrostatic forces are transformed into a relatively small friction torque at the gate hinges. These gates are usually used as safety gates at upper ends of locks or for low lift locks where their height and therefore weight can be kept within manageable limits. These gates are relatively expensive, for high water heads, because of high weight per unit height and additional concrete works required to accommodate them in the open position.

The loads on a sector gate are similar to those of a sliding gate and are easily predictable. A version of the sector gate known as the taintor gate has also been used for barge canals. However, it is usually limited to use as filling or emptying valves for locks.

Mitre gates, Figure 2.4, is the most economical and favoured design for medium and high lift locks. The design approximates the thin arch principle and some gates have in

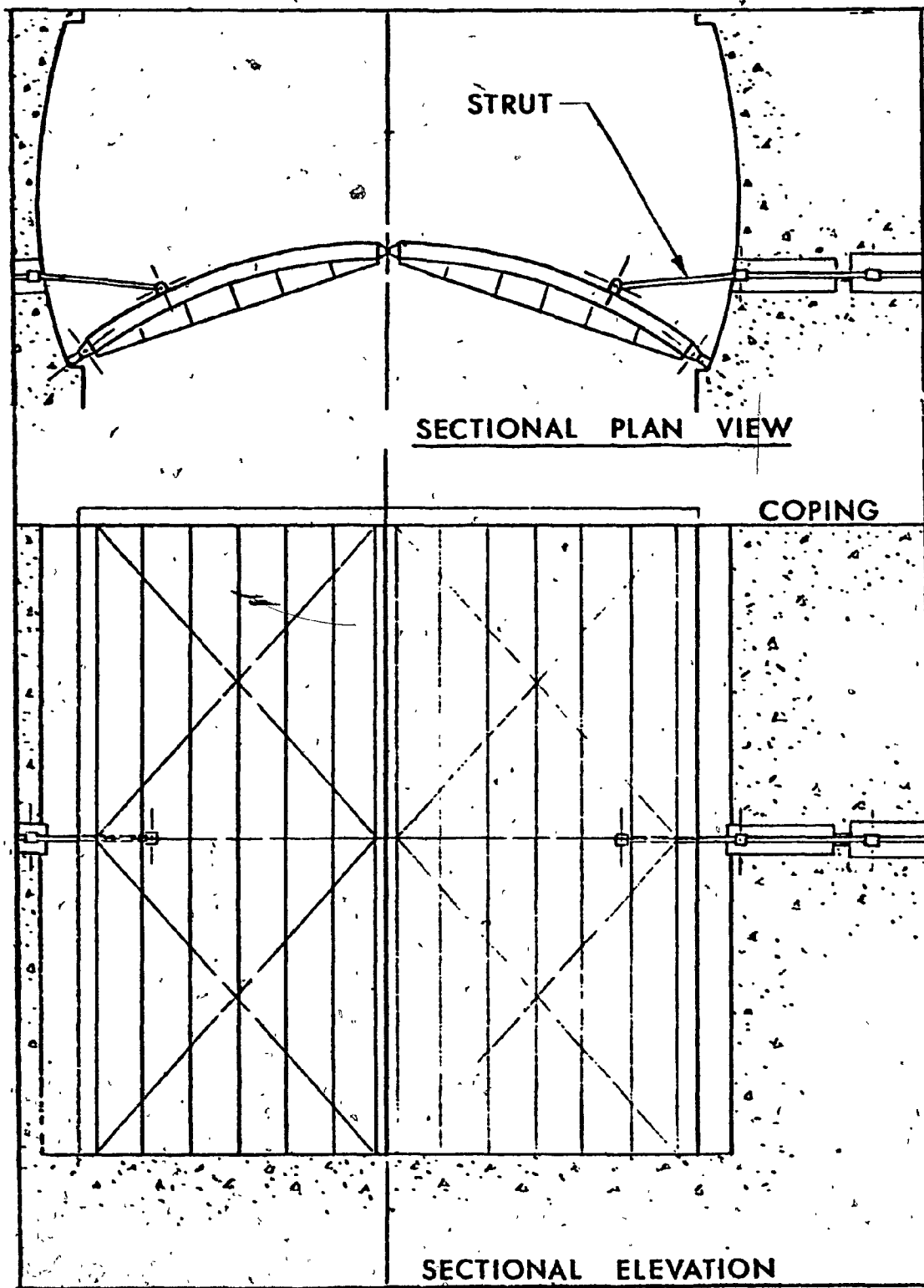


Figure 2.4 Mitre Gate [4]

fact been built to this shape [4]. The configuration entails the least amount of concrete work to support the gate and allows for the gate to be protected by timbers, or other type of fendering, from damage by passing vessels. Other good features include the relative ease with which damaged gates can be replaced and the path of the gates can be cleared from ice during cold weather navigation. On the negative side, the operation of mitre gates is highly sensitive to water resistances, due to the fact that its full submerged surface area displaces water during the pivoting operation. High loads can be imposed on the gate by surges of water around the lock. A difference of water levels between the two sides of the gate leaf by 0.2 m will make most gates inoperable [5]. The loads on mitre gate drive mechanisms are relatively difficult to predict due to the variation in amplitude and frequency of water surges acting on the gates.

2.2 Drive Mechanisms for Gates

In general the gate drive mechanisms can be subdivided into the following categories:

- 1) Wire rope or winch type, by which the gate is pulled in both operating directions or lifted and dropped by gravity.
- 2) Strut type, by which the gate is pushed and pulled.

iii) Other types such as a combination of wire rope and strut into a single unit.

Some examples of the mechanisms, including hydro-mechanical are shown applied to mitre gates in Figures 1.2, 2.4 and 2.5.

2.3 General Criteria for Gate Drive Mechanisms

The criteria, below, are for drive mechanisms operating mitre gates only. However, the variables which have to be considered in the design of a drive for a mitre gate will include most of the important variables affecting drives for other navigation lock gate configurations. Hence, the criteria outlined for the mitre gate drive can be applied without loss of generality to other types of lock gate drives.

2.3.1 Capital and Operating Costs

In considering the capital cost of a type of machine, one has to take into account the cost of housing the machines. The housing should involve the least amount of concrete work in the monolith and should not obstruct visibility or traffic around the lock and should provide easy access to the machinery.

The operating costs, apart from materials and maintenance labour, must allow for the downtime of vessels which can be delayed in the canal. Currently the cost of an average idle vessel in the St. Lawrence Seaway is approximately \$5,000/24 hrs. It follows that the machine should be simple

and easily understood and such features as submerged components which have to be maintained by divers should be avoided. Generally, the number of trades involved in maintenance should be a minimum.

2.3.2 Geometrical and Space Considerations

In general the highest load torque on the gate occurs, around the fully open and fully closed gate positions. It is desirable that the machinery have the maximum mechanical advantage in these parts of gate travel. A design satisfying this requirement is illustrated in Figure 1.2. The high mechanical advantage complements the requirement to keep the gate velocities low at the start and closing of an operating cycle.

Loads produced by a drive mechanism on a gate have to be compatible with the gate structure. For example the load on a mitre gate is generally applied by the water at a low elevation of the gate, while the driving force is usually applied at the top of the gate to avoid submerging machinery components. This gives rise to large diagonal twisting moments across the gate.

2.3.3. Compatibility with other Lock Machinery

The gate drive mechanisms should be suitable for remote operation and interlocks with other lock operating mechanisms such as drives for filling and dumping valves. The control system should have a minimum number of interfaces between the various powering and control media.

2.3.4 Overload Protection

The gates can on occasion be suddenly stopped in their path by debris such as floating timbers and very frequently by ice during the cold season. The machinery must, therefore, be provided with protection against damage on these occasions. This can be achieved by providing shear connections, slip-friction clutches and relief of pressure in hydraulic machines. Rendering is preferable to shearing and replacement of connections because it entails no delays to navigation and also it acts as an energy absorber in case of a load reversal on the gates created by water surges in the lock. Absorbing the surge energy ensures that a gate is not carried away by the water and slammed against its end position stops, with consequent danger of twisting and damage.

2.3.5 Gate Locking

The machines must be capable of locking the gates at any position of their travel. The lock must be sufficiently positive to prevent the gates from creeping from open position into the path of a vessel and to allow maintenance work on the gate without any dangerous movements.

2.3.6 Power Requirement

The actual power consumption of the machines is of little significance, since the average running time of the machines is under 1 hour/day. It is the peak power which establishes the utility's billing rate, and the capital cost of the machinery by determining the minimum size of machinery components..

A flat power curve throughout the operating cycle should be the ideal goal of the design since this would ensure the shortest operating time per \$ of capital expenditure and the lowest power cost.

2.3.7 Loads on Gate Machinery

The loads normally consist of water resistances to movement of the gate, random water loads created by surges due to passing vessels and/or lock operations, mechanical friction, wind and inertia of moving gates. Other loads that resist the motion of the gate as cited in Section 2.3.4 must also be taken into account.

A more detailed description of the loads is presented in Chapter III.

2.4 Hydro-Mechanical Gate Drive Mechanisms

The drives are of two types. Those employing cylinders as actuators, exemplified by Figure 2.6 and those employing hydraulic motors, exemplified by Figure 1.2.

In drives utilizing the cylinder, the cylinder rod becomes the strut. The drives have the advantages of simplicity and relatively low initial cost. However, they can introduce undesirably high forces onto the gate structure due to the short gate radius at which the rod is usually applied. Also, it is difficult to lock the cylinder mechanically when it is required to prevent gate movement

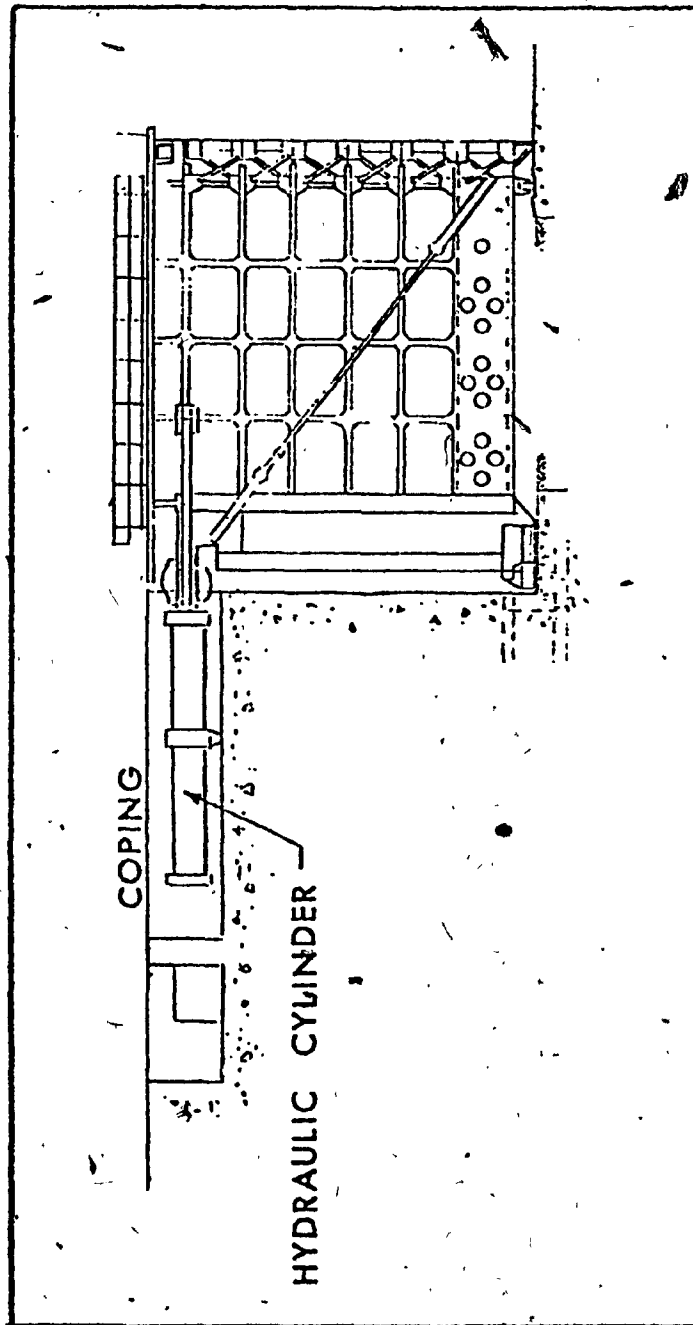


Figure 2.5 Hydro-Mechanical Gate Drive [4]

due to leakage of oil past seating faces of the hydraulic components.

The drives utilizing a hydraulic motor overcome the disadvantages listed for the cylinder type. The load can be applied to the gate at any point or angle it is desired by selecting a suitable arrangement of strut links. Also, a simple band brake around the motor can lock the gate in any position desired.

CHAPTER III
SIMULATION OF HYDRO-MECHANICAL
MITRE GATE DRIVES

3.1 Preamble

It has been established by experiments [6] that the prototype hydro-mechanical drive discussed in Chapter I performed well and satisfied all the design requirements. It is hereafter assumed that this particular drive design can be adapted, after optimization, for use throughout the St. Lawrence Seaway and waterways of similar magnitude. The simulation that follows is of a mitre gate drive whose mechanical side is shown in Figure 1.2, and whose hydraulic circuit modification consists of driving the hydraulic motor by a single constant power pump instead of the two pumps as in the prototype. A schematic representation of the drive to be simulated is shown in Figure 3.1(a). The single pump circuit has in fact been the original design of the prototype but had to be abandoned due to unavailability, in the required time of a single pump of the required size.

The purpose of the simulation is to gain a better understanding of the interrelation of the various loads on the gates, to optimize the power of the gate drive mechanism and to estimate the maximum range of gate closing times when abnormal water surging takes place in the lock.

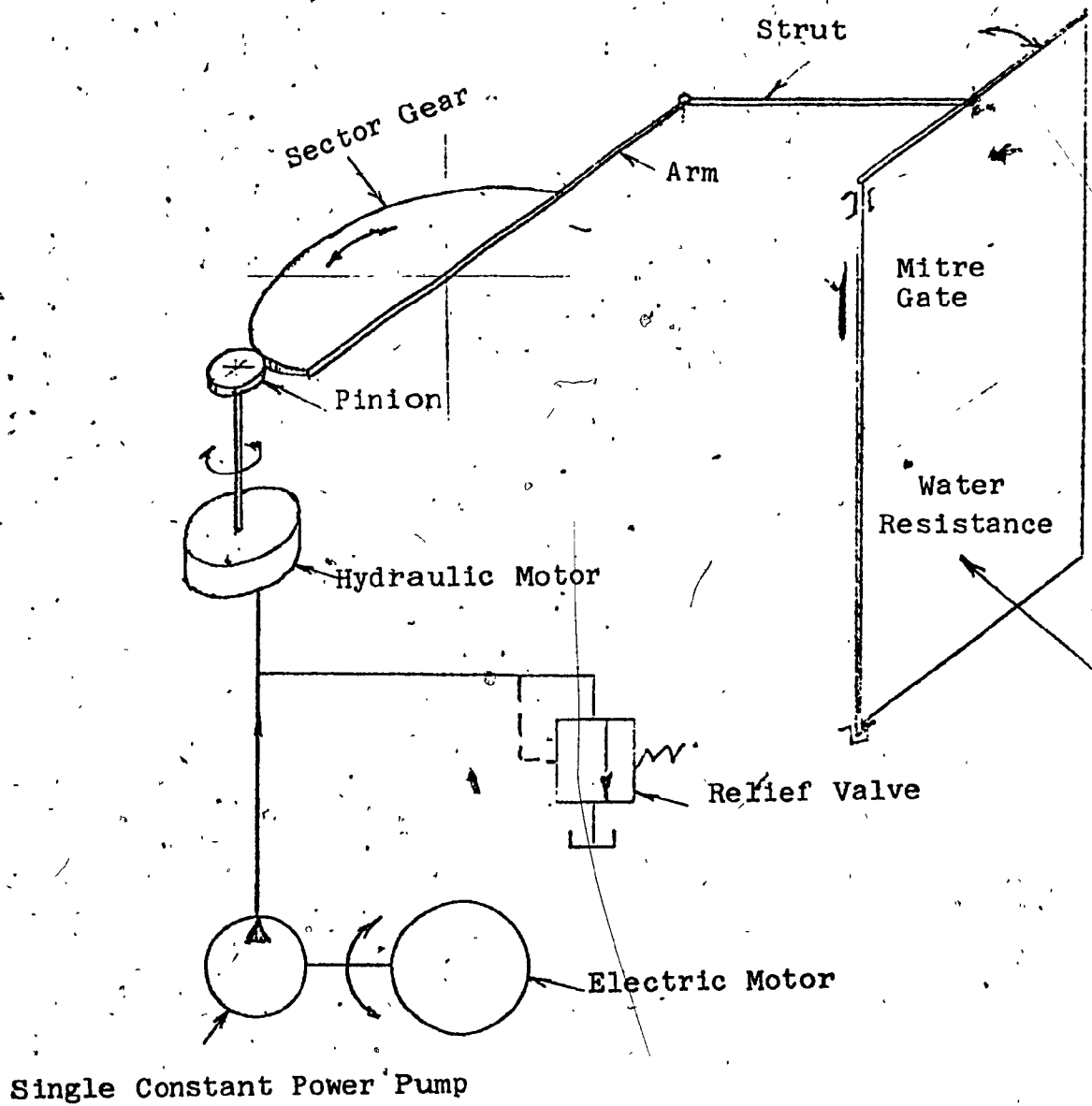


Figure 3.1(a) Schematic Representation of Simulated Drive

3.2 General

The loads that act on the mitre gates and the assumptions made in the formulation of the governing equations describing the operating characteristics of the gate are discussed. The Power Bond Graph technique [7,8] is utilized in the construction of the mathematical model of the gate mechanism. Using the Power Bond Graph, the flow continuity and compatibility equations describing the gate mechanism can be directly formulated.

3.3 Loads on Mitre Gate Drive Mechanism

The gate drive has to overcome both external and internal loads acting on it. The nature of the loads and their relative importance are discussed below.

3.3.1 Frictional Load

Mechanical friction in gate pivots and gate drive mechanism links can be assumed as an equivalent constant gate torque with the gates in motion. A higher starting friction can be assumed at the extreme positions of the gate, however, this does not seem appropriate since the various members of the machinery and gate have some coupling compliance before the full torque is developed on the gate. Also, the only use of such a model would be to check whether sufficient torque exists to overcome the friction.

3.3.2 Wind Load

The wind load very much depends on the lock configuration and the prevailing wind direction. Hence a maximum load value for wind can only be assumed in the mathematical formulation.

In North America it is customary to stop navigation at wind gusts of approximately 50 km/hr, and this low speed combined with the fact that the gates are sheltered by the surrounding ground makes wind load a negligible influence on gate drives. In the St. Lawrence Seaway the worst possible combination of wind forces, during navigation, would be less than 20% of the water load. Therefore, no account will be taken of wind in the model for normal operation.

3.3.3 Water Surging in Lock

Water surges are often created by passing vessels and during lock emptying operations. The surges can roll into a lock and bounce back with the water head reversed. Liou [9] has estimated the magnitude and frequency of surges in a lock in the St. Lawrence Seaway. The mathematical model of the gate drive mechanism presented in this dissertation includes the effect of water surging in the lock.

3.3.4 Effect of Inertia Load on Gate

The mass of a typical gate on the St. Lawrence Seaway is approximately 225,000 kg. and its effect on the model cannot be ignored. In the machinery of the type shown in Figure 1.2, the effect of inertia during acceleration and deceleration is softened by the high mechanical advantage during these periods due to the geometry of the strut mechanism.

3.3.5 Water Resistances

These resistances are particularly important in the case of mitre gates where, as in the case of a ship, viscosity and wave resistances play a part.

Lejeune [10] established a generalized relationship between the angular speed of a gate and the resisting water torque. He obtained a good correlation with model tests carried out to prove the validity of the relationship. However, the model tests conducted were oversimplified and did not represent truly conditions encountered in canals. The formulation when compared with experimental results obtained from gates on the St. Lawrence Seaway proves itself unsatisfactory. The actual resistance of gates is highly dependent on the shape and construction details and extremely sensitive to the angle of opening of the gate at which the resistance is measured. It was also found that even a very slight change in the angle of opening of the gate has a pronounced effect on the water resistance at the point where the gates are almost fully closed [11].

Tests conducted by the U.S. Army Engineer Waterways Experimental Station [11] show that the variables that affect the water resistances of mitre gates are:

- a) Operating time;
- b) Submergence of gates;
- c) Bottom clearance;
- d) Degree of synchronization of movement of a pair of gates;
- e) The kinematic characteristics of the operating machinery;
- f) Structural details of gates.

The model tests referred to above were conducted with a model of an actual gate installation and built to a scale of 1:20. The model represented the gate installation in great detail. Since the St. Lawrence Seaway gates and drives are very similar to those model tested, the relationships obtained from the tests can be used with considerable confidence in the mathematical simulation.

3.3.6 Other Loads

Other loads which would influence gate machinery performance are:

- a) Errors in operation of lock filling valves which would result in the gates being carried away towards the closed position by a wall of water [12].

b) Floating debris or ice hitting gates.

Because of the infrequent occurrence of the above mentioned loads, they are not to be included in the mathematical modeling of the gate machine.

3.4 Assumptions

In order to consider only those system characteristics that have primary influence on the performance of the gate operation, the following assumptions are made:

- (1) The breaking valves, and check valves function only in abnormal situations and can be ignored in a normal operation;
- (2) A single pressure P_a is assumed throughout the system after the fluid leaves the pump. This is justified since line and valve pressure losses should be under 5% of P_a ;
- (3) The power output of pumps is constant;
- (4) ΔP or pressure drop across the relief valve is negligible;
- (5) Capacitance effects in the hydraulic circuit part of the gate drive are ignored. The response of the gate to pressure transients in the hydraulic circuit should be of little interest to a gate drive designer;

(6) No allowance is made for the time taken to operate valves and starting or shutting down the system. The effects produced appear relatively unimportant in gate drive design.

(7) The strut by which the gate is pivoted is assumed rigid when in fact it is spring loaded in both the pulling and pushing direction. The effect of the spring is to limit the value of the ratio of torque on the gate to the torque on the hydraulic motor to a maximum of 30, during the commencement and termination of a gate operation. The above figure has been established experimentally and will be incorporated into the simulation.

(8) The water head difference across the gates produced by water surging in the lock is assumed at 0.1524 m at its maximum amplitude and the surge period at 180 seconds. These values were suggested by Liou [9] for one of the St. Lawrence Seaway locks.

(9) The effect of high winds is ignored since navigation in the St. Lawrence Seaway stops at wind velocities of 48 Km/h. The effect of occasional floating ice is also ignored since it is unpredictable.

(10) In interpolating the model test results for gate water load, the gate wave resistance is assumed to be the only resistance [11]. Since the interpolation takes place over narrow ranges, and the wave resistance is preponderant over the range of speeds at which the gates are operated, errors should be negligible.

(11) At any given angle of gate opening, the change in water resistance is assumed to be proportional to the change in the square of the velocity of the gate. This assumption implies that over the range of gate speeds contemplated in the modelling, the patterns of water movement relative to the gate are the same at each given angle of gate opening.

3.5 Mathematical Modeling of Mitre Gate Drive

In order to obtain the mathematical equations, the hydraulic circuit with lines and components as shown in dark lines in Figure 3.1 is considered. It can be seen that the hydro-mechanical gate drive is controlled by a single pump and its associated valves. The idea of operating a mitre gate using a single pump unit was the original intention of The St. Lawrence Seaway Authority at the time of converting to a hydro-mechanical drive from the existing hydro-electric drive. However, due to unavailability of a single pump with 50 HP, a two-pump hydro-mechanical drive was built. In this dissertation, the simulation of a single pump controlled hydro-mechanical drive is carried out to obtain the optimal performance characteristics.

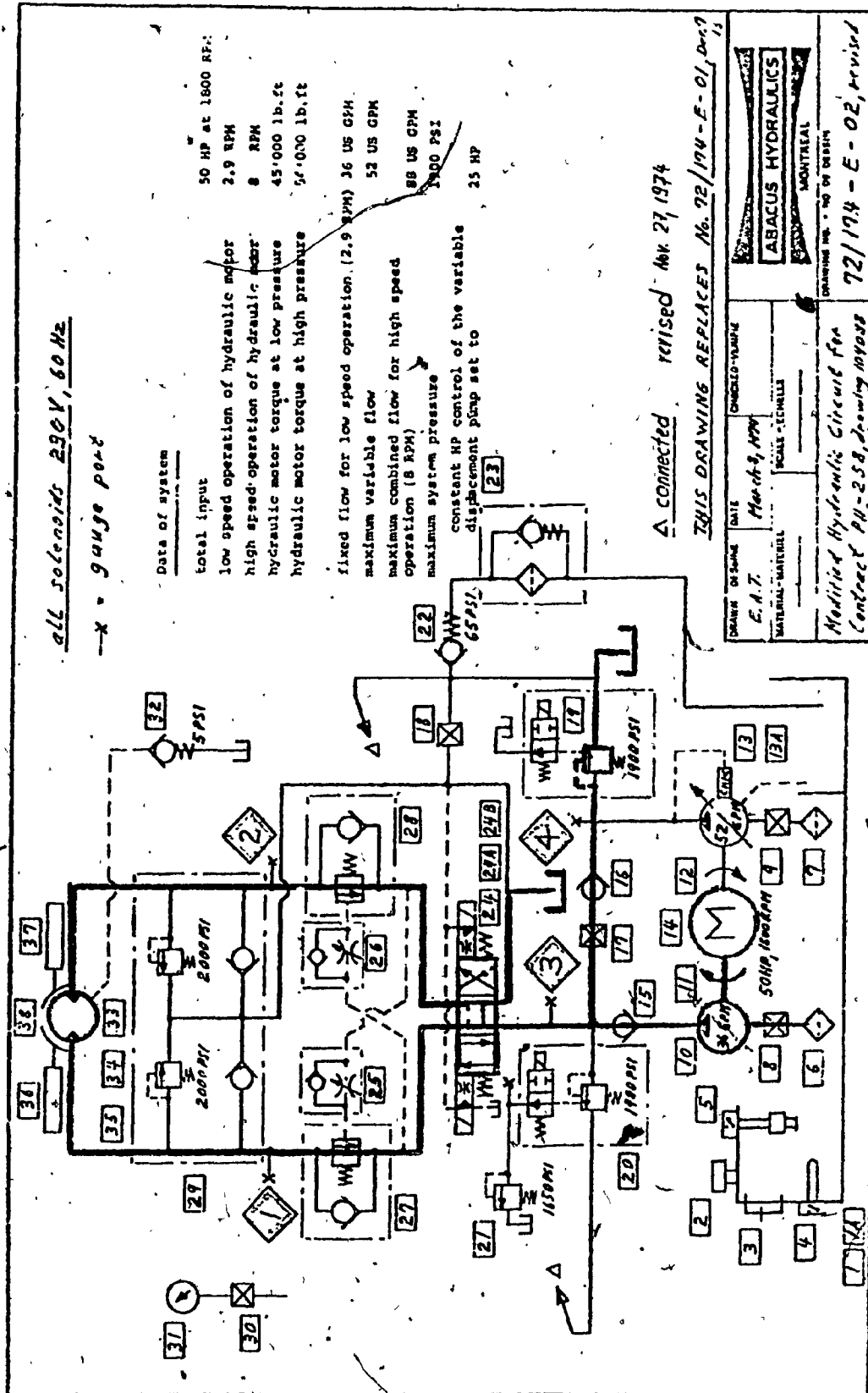


Figure 3.1(b) Simulated Circuit

3.5.1 The Governing Equations

The governing equations of the hydro-mechanical drive are formulated using the power bond graph technique. A general description of the power bond graph method is illustrated in Appendix A. The power bond graph of the hydro-mechanical gate drive is shown in Figure 3.2. Using the bond graph diagram, the following equations governing the gate drive mechanism are obtained.

The power at the pump shaft and the system input variable is:

$$HP_p = 746 \text{ HP} \quad (3.1)$$

Since the hydraulic pump is of the constant power type the system input flow is

$$Q_1 = HP_p / P_1 \quad (3.2)$$

The mechanical loss across the pump is given by

$$P_f^p = P_1 (1 - N_{\text{mech}}^p)$$

where N_{mech}^p , the mechanical efficiency of the pump is taken at 93% as specified by Brueninghaus for their pump model 125EZ1 RP1/R1120.

Hence, the pressure loss becomes

$$P_f^p = 0.07 P_1 \quad (3.3)$$

The system pressure, P_a is given by

$$P_a = P_1 - P_f^p \quad (3.4)$$

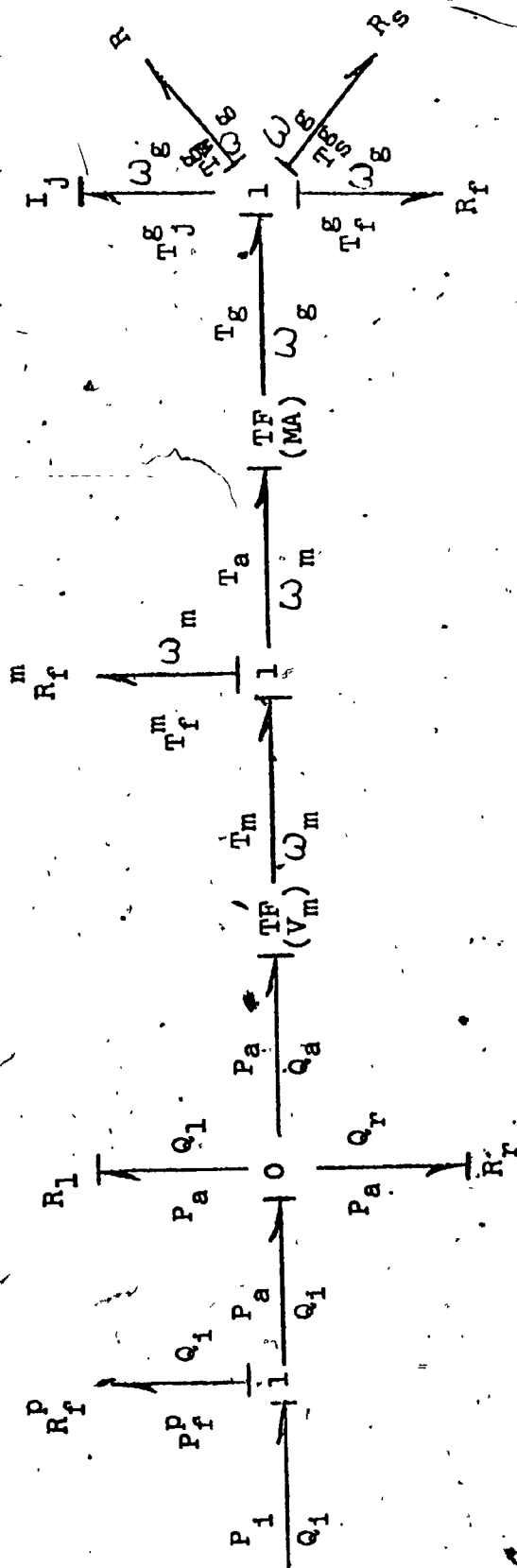


Figure 3.2 Power Bond Graph

The flow to the hydraulic motor Q_a is obtained by the continuity equation as

$$Q_a = Q_1 - Q_l - Q_r \quad (3.5)$$

The combined leakage flow past the hydraulic pump and motor can be stated as

$$Q_l = (K_1 + K_2) P_a$$

where K_1 is the leakage constant for the pump obtained from the Brueninghaus catalogue and K_2 is the corresponding constant for the Hagglunds hydraulic motor type A8385L. The leakage constants can be combined in this linear relationship because the flow is laminar and a single system pressure P_a has been assumed.

The system leakage loss is given as

$$Q_l = 34.62 \times 10^{-12} P_a \quad (3.6)$$

Leakage past relief valve Q_r , is given as

$$\begin{aligned} Q_r &= Q_a - N_V^m \cdot V_m \cdot M A \cdot \omega_g & \text{at } P_a > 13.1 \times 10^6 \\ &= 0 & \text{at } P_a \leq 13.1 \times 10^6 \end{aligned} \quad (3.7)$$

The volumetric efficiency of the Hagglunds motor N_V^m is rated by the manufacturer at 94%. The volume constant of the motor V_m is given by Hagglunds as 0.00607. The relief flow becomes

$$\begin{aligned} Q_r &= Q_a - 0.0057 M A \cdot \omega_g & \text{at } P_a > 13.1 \times 10^6 \\ &= 0 & \text{at } P_a \leq 13.1 \times 10^6 \end{aligned}$$

The equation for relief valve flow is obtained by considering continuity; the flow is the difference between the flow Q_a and the flow into the hydraulic motor. The motor is rigidly coupled to a mitre gate of high inertia and the gate will continue on its path, for some time, even though the relief valve is lifted. When the kinetic energy of the gate is being dissipated, part of the flow Q_a is taken into the motor and the remainder passes through the relief valve.

The torque at the shaft of the hydraulic motor T_m , can be stated as

$$T_m = P_a \cdot V_m \quad (3.8)$$

The motor constant can be considered as

$$V_m = A_p \cdot R_p$$

where A_p is an equivalent motor piston area at radius R_p turned through an angle of one radian. Then, the units of V_m are those of a moment of area.

The hydraulic motor speed is given by

$$\omega_m = Q_a / V_m \quad (3.9)$$

The frictional torque on the hydraulic motor due to mechanical friction in the motor and the mechanism linking it with the mitre gate is

$$T_f^m = T_m (1 - N_{\text{mech}} \cdot N_d) \quad (3.10)$$

The mechanical efficiency of the motor, N_{mech} is given by Hagglunds, the motor manufacturer, as 97%. The efficiency of the linking drive, N_d is calculated as 94% by multiplying standard component efficiencies for the drive [13].

The output shaft torque at the motor T_a , is

$$T_a = T_m - T_f^m \quad (3.11)$$

Referring to Figure 3.3, the mechanical advantage between the hydraulic motor torque and the torque on the mitre gate can be written as

$$\begin{aligned} MA &= K_3 \frac{d}{d\theta} (2\pi - A - B) \\ &= K_3 \frac{d\varphi}{d\theta} \end{aligned}$$

where K_3 is a constant relating the gear ratio between the motor shaft mounted pinion and the gate drive sector gear.

$\frac{d\varphi}{d\theta}$ is the inverse of the velocity ratio between the gate and the hydraulic motor. For the St. Lawrence Seaway drives, the equation becomes

$$MA = 10 \sin \theta \frac{-0.006825 X^{-3} + 0.35 X^{-1} + 0.3087 X^{-3} + 0.6625 X^{-1}}{[1 - (0.01365 X^{-3} + 0.7 X)^2]^{1/2} [1 - (0.6175 X^{-1} + 1.325 X)^2]^{1/2}}$$

$$\text{where } X = (1 - \cos \theta)^{0.5}$$

and θ varies from 0.6340 to 1.882 for gate closing and 1.882 to 0.6340 for gate opening.

The expression for the total torque on gate is

$$T_g = MA \cdot T_a \quad (3.13)$$

The torque compatibility at the gate gives

$$T_g = T_j^g + T_w^j + T_f^g + T_s^g \quad (3.14)$$

The speed of the gate can be expressed as

$$\omega_g = \omega_m / MA \quad (3.15)$$

where MA is the inverse velocity ratio.

Also, the gate speed is equal to the time integral of its angular acceleration written as

$$\omega_g = 1/I \int_0^{T_{now}} T_j^g dt$$

Substituting for the moment of inertia, I of the gate on the St. Lawrence Seaway gives

$$\omega_g = 1/14.71 \times 10^6 \int_0^{T_{now}} T_j^g dt \quad (3.16)$$

The gate friction torque is a constant due to resultant forces on gate hinges and applicable friction coefficients [5]. By calculation the value is found to be

$$T_f^g = 87000$$

The water torque on the gate is calculated from model test results developed by the U.S. Army Waterways Experimental Station [11]. Assumption No. 11 in Section 3.4 is necessary to apply the model test data to the St. Lawrence Seaway gates. The assumption allows normalizing the model torques with respect to ω_g^2 for any position of gate. Normalization is necessary due to the model drive links being of slightly different proportions than in the Seaway drive.

Figure 3.4 illustrates the model test results which are most applicable to the Seaway gates and drives. Table 3.1 shows the plotted results normalized for given angular position of gate, in the form of the parameter,

$$P_t = \frac{T_w^g(\text{model})}{\omega_g^2(\text{model})} \quad (3.17)$$

Values for gate positions between those given in the table are interpolated.

The expression for water torque on the gate can be written as

$$T_w^g = K_4 \cdot P_t \cdot \omega_g^2 \quad (3.18)$$

where $K_4 = 651083$ is a constant obtained, through dimensional analysis [14], which converts model results to prototype scale.

The time from start of a gate cycle is given by the integral

$$T_{\text{now}} = \int_{\theta_1}^{\theta_2} 1/\omega_g d\theta \quad (3.19)$$

Water surges acting on mitre gates are not a function of the gate opening. They are caused by independent phenomena such as passing vessels or operation of other lock mechanisms. The torque produced on the gate, however, is the result of the area the mitre gates project towards the surges that are coming along the longitudinal centre line of the lock and are proportional to the projected areas [15]. The obstacle of the gate results in a water head difference from one side of the gate to the other creates a resisting torque on the gate. Section 3.4 states the assumed values of the amplitude and period of the static head difference on the gates.

The static pressure due to surge on the gate is

$$P_h = \rho \cdot a \cdot \sin \omega t \sin (\theta - 0.634)$$

Where ω is calculated from the surge period and the constant 0.634 represents the gate angle in the fully open position.

Table 3.1 Values of Parameter P_t

θ (Deg)	θ (rad)	g^2 (rad/s ²)	Closing		Opening	
			T_W^g (Model)	P_t	T_W^g (Model)	P_t
36.33	.634	.0043	52	1	13.0	4100
37.47	.654	.006	52	11755	11.5	2600
38.86	.680	.008	32	5425	9.7	1645
39.99	.698	.0093	16	2333	9.5	1385
42.97	.750	.0122	14.3	1590	7.0	777
44.98	.785	.014	14.0	1356	7.5	727
50.02	.873	.0175	11	823	9.5	736
59.99	1.047	.0225	12.5	753	10.0	602
70.02	1.222	.0247	13.5	742	10.5	576
79.99	1.396	.024	14.6	825	13.0	735
90.01	1.571	.0203	18	1203	15.0	1002
97.41	1.700	.0157	24.3	2100	16.4	1417
99.99	1.745	.0135	25.3	2542	17.6	1769
104.34	1.821	.0093	32.3	4710	24.5	3572
104.97	1.832	.0085	29.5	4708	26.5	4229
106.23	1.854	.0065	24.5	5112	27.0	5634
107.83	1.882	.0034	17.5	6981	27.0	1

Note: P_t values in table have been multiplied by 1.3563 to convert to S.I. units.

The time from the start of a surge at the mitre gate t , is given by

$$t = T_{\text{now}} + b$$

where b is the lag in time between the start of a gate operation and the start of a surge at the gate. The constant b can take on any value within the surge period of 180 seconds

$$0 < b \leq 180$$

The general expression for the surge torque is

$$T_S^g = P_h \cdot A \cdot R$$

assuming the surge amplitude and period as stated in Section 3.4, and from the dimensions of the submerged portion of the gate, the expression for T_S^g becomes

$$T_S^g = 1436085 \sin 0.0349t \sin (\theta - 0.634) \quad (3.20)$$

The above set of equations (3.1) - (3.20) completely describes the behaviour of the hydro-mechanical gate drive using a constant power pump.

3.7 Digital Computer Simulation

The simulation is carried out on a digital computer, Burroughs model B2500 using Fortran IV language.

The input variables are a set of values of power input into the constant power pump and a set of initial values and ranges of applicable variables. Relevant variables are calculated at discrete time intervals from the start of gate operation. Gate closing and opening operations are simulated for a set of power input values ranging from 10 HP to 50 HP in steps of 5. For each of the power inputs, printouts of variables are obtained at time intervals ΔT_{now} , ranging from 0.01 to 0.2 seconds. The simulation assumes normal operating conditions with no water surges in the lock. Representative values of the variables investigated are shown in Tables 4.3 and 4.4 and Figure 4.9. The program listings for gate opening and closing are attached in Appendix B.

The effect of water surges is investigated for a gate drive with a power input of 25 HP - the power established as most economical in the cost optimization described in Chapter V. The effect on gate closing times is investigated for a surge of fixed amplitude and frequency. Gate closing times are calculated for surges starting at the gate with various time lags after the start of gate closing. The results of this simulation are shown in Table 5.2. The program listing is enclosed in Appendix B.

2

CHAPTER IV

PERFORMANCE CHARACTERISTICS OF THE PROTOTYPE HYDRO-MECHANICAL GATE DRIVE ON THE ST. LAWRENCE SEAWAY

4.1 General

This chapter will describe the conversion of an existing mitre gate drive on the St. Lawrence Seaway from electro-mechanical to hydro-mechanical mechanism. Design constraints imposed by the existing mechanism will be described briefly followed by a discussion of the procedures used to estimate the performance of the modified drive. The operation of the modified drive will also be described during a complete gate operating cycle. A section will be devoted to tests carried out on the modified drive, including instrumentation and measurement procedures used.

The chapter will include a discussion on the correlation of results obtained from the tests and those obtained from the computer simulation described in Chapter III.

4.2 Design Constraints Imposed on Hydro-Mechanical Drive Mechanism

The existing electro-mechanical drive, Figure 1.2, was designed to withstand stresses corresponding to a peak torque which, due to the lengths of the mechanism links chosen, occurred just before the gates reached their fully open position. In converting to a hydro-mechanical drive, it became possible to increase the maximum torque capacity of the mechanism over most of the pivoting angle of the gate.

This was achieved by maintaining the hydraulic system pressure at a level corresponding to the original peak torque, in a 3° gate pivoting interval adjacent to the gate fully open position. During the remainder of the gate pivoting angle, the relief pressure was boosted to correspond with a torque substantially higher than in the original drive. This design approach approximates the ideal utilization of the mechanical strength of the existing components, i.e. if this machinery can maintain maximum hydraulic system pressures throughout the cycle, regardless of the velocity of the mitre gate and therefore the pump delivery, the shortest operating time is possible.

By assuming water resistance as the dominant load on the gate, it is possible to estimate the maximum power required for the hydraulic drive and its maximum operating time. From Lajeune's study [10], the load due to water resistance was considered to be proportional to the square of the gate velocity. Using this relationship, the maximum power required for the gate operation was calculated to be 150 HP. However, the power of the existing electro-mechanical drive was only 20 HP with an operating time of 72 seconds. Hence an input power of 50 HP was selected instead of the ideal 150 HP as the power required for operating the mitre gate with a hydro-mechanical drive.

The operating time with this arbitrary power input, was estimated from the power consumption measurement taken on an electrical motor drive for identical gate drives. A typical power measurement curve is shown in Figure C1 in Appendix C. The power curves were replotted as torque vs time, as shown in Figure 4.1 using motor characteristics.

In order to predict the behaviour of the drive after converting to a hydro-mechanical drive mechanism, the above torque vs time relationship has to be modified to suit the power input of the hydraulic motor. A typical hydraulic motor characteristic is shown in Figure 4.2 as a curve relating hydraulic motor R.P.M. against system pressure. A further requirement is that the relationship between motor speed and time should be known for the electro-mechanical drive. This was determined experimentally for a typical gate and is shown in Figure 4.3. Through the common time base of Figures 4.3 and 4.1, gate torques for particular motor speeds are known.

Considering water resistance as the predominant load on the gate and assuming it to be proportional to the square of the gate speed, the following instantaneous relationships between the electro-mechanical and hydro-mechanical drives can be written:

$$\frac{\Delta T_g^e}{\Delta T_g^h} = \left(\frac{\Delta \omega_g^e}{\Delta \omega_g^h} \right)^2 = \left(\frac{\Delta T_{now}^h}{\Delta T_{now}^e} \right)^2 = \left(\frac{\Delta \omega_m^e}{\Delta \omega_m^h} \right)^2 \quad (4.1)$$

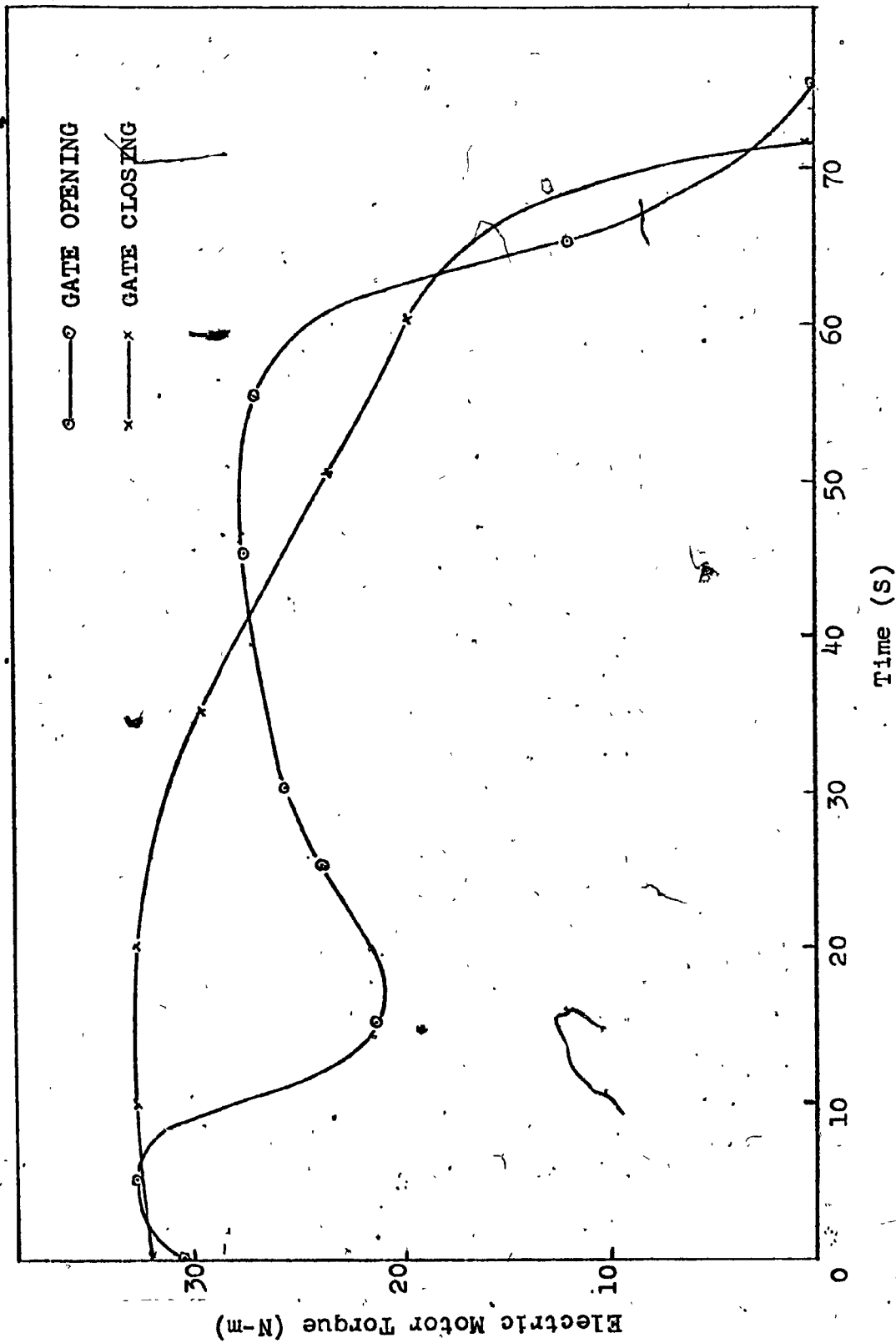


Figure 4.1 Torque Characteristics of an Electro-Mechanical Gate Drive

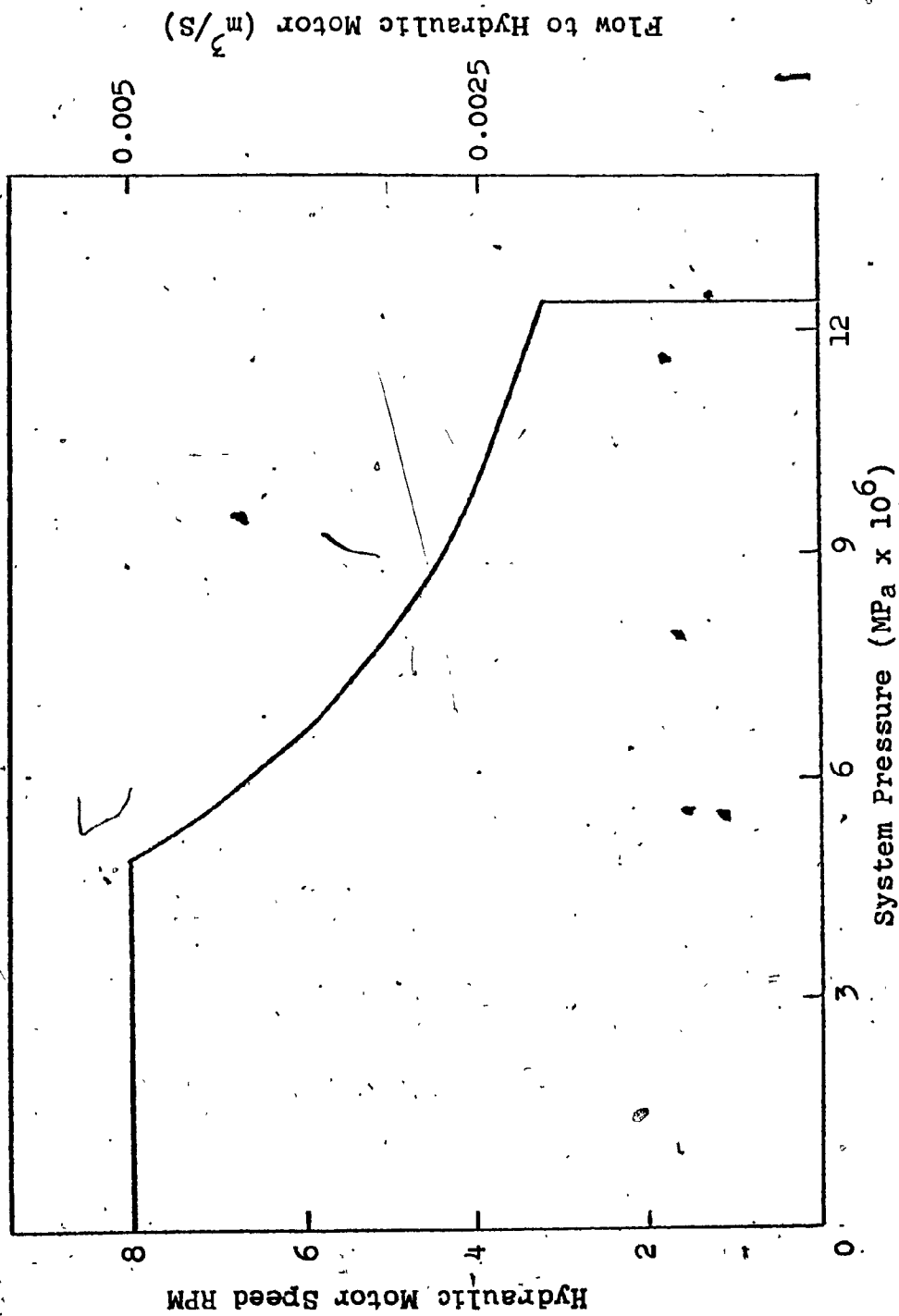


Figure 4.2 Hydraulic System Flow VS System Pressure

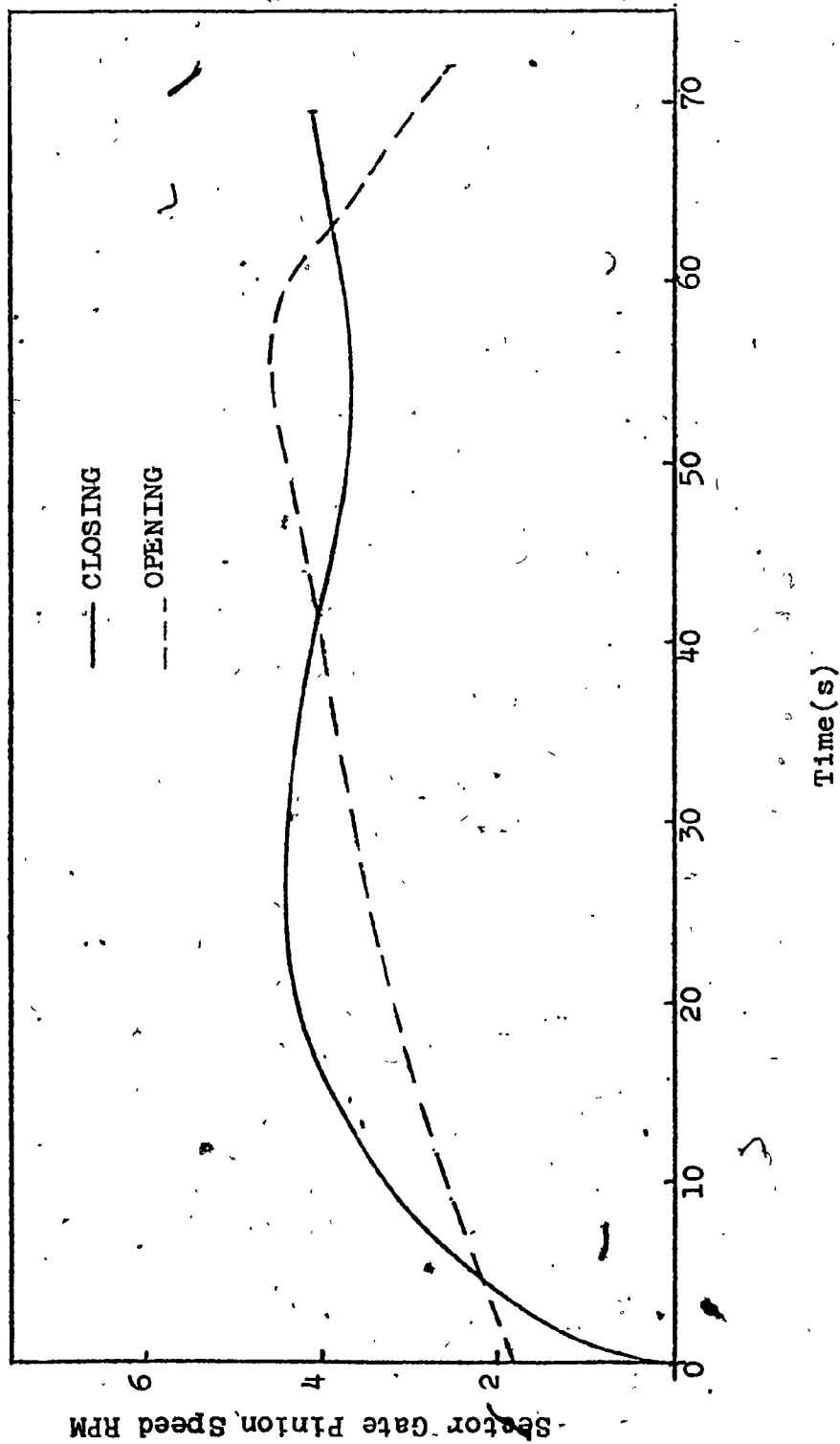


Figure 4.3 Sector Gate Pinion Speed Vs Time

From equation (4.1), the following two equations can be written:

$$T_{\text{now}}^h = \sum T_{\text{now}}^e \cdot \left[T_g^e / T_g^h \right]^{\frac{1}{2}} \quad (4.2)$$

and

$$T_{\text{now}}^h = \sum T_{\text{now}}^e \cdot \omega_m^e / \omega_m^h \quad (4.3)$$

Equation (4.2) would be sufficient to find the gate operating time T_{now}^h , if T_g^h could be maintained at a constant maximum value. This, however is impossible due to the arbitrary limitation of power of the hydraulic drive to 50 HP.

From equation (4.1) it can also be written:

$$\left[T_g^e / T_g^h \right]^{\frac{1}{2}} = \frac{\omega_m^e}{\omega_m^h} \quad (4.4)$$

Since the values of T_g^e and ω_m^e are known for an electro-hydraulic drive from Figures 4.1 and 4.3, through the common time base, the relationship of T_g^h and ω_m^h can be obtained from Figure 4.2 by converting pressure to torque.

If the time scale in Figure 4.1 is divided into small intervals T_{now}^e and the mean values of T_g^e and ω_m^e found for each interval, there will exist a point on the locus in Figure 4.2 which will give values of T_g^h and ω_m^h that will satisfy equation (4.4). Once these values are known for each interval ΔT_{now}^e , the gate operating times can be obtained by using equation (4.2) or (4.3).

Utilizing the above relationships it is also possible to estimate T_g^h and ω_m^h with respect to time for the operation of the hydro-mechanical drive. The estimated relationships are shown in Figures 4.4 and 4.5.

4.3 Functional Description of the Hydraulic Circuit

Functionally the circuit was designed to do the following:

Gates Closing Cycle

1. The gate to leave the gate recess with hydraulic motor delivering a torque of 61000 N-m and running at a reduced speed of 3.5 R.P.M. The speed is reduced to eliminate any vibration of the gate structure and is achieved by limiting the motor supply to the constant delivery pump.
2. After the gate has pivoted between 3° to 5° the motor torque is increased to a maximum of 73250 N-m and the gate is driven at maximum possible speed. The increase in torque is achieved by raising the relief pressure of the circuit. The increase in speed is the result of switching the delivery of the constant power pump to drive the hydraulic motor along with the constant delivery pump.
3. Just before the closed position the hydraulic motor speed is again reduced to 3.5 R.P.M. by cutting out the delivery of the constant power pump.

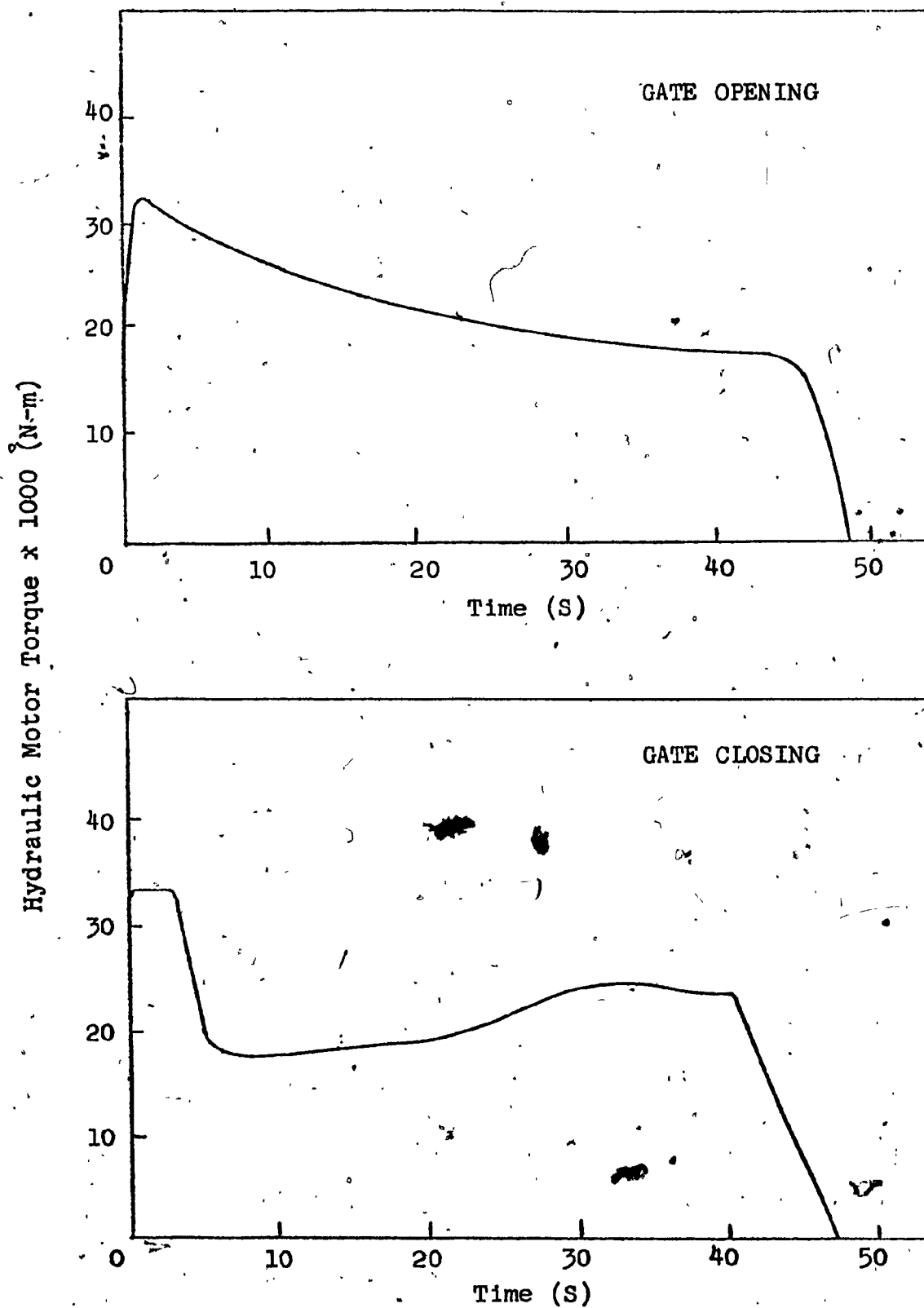


Figure 4.4 Hydraulic Motor Torques Vs Time

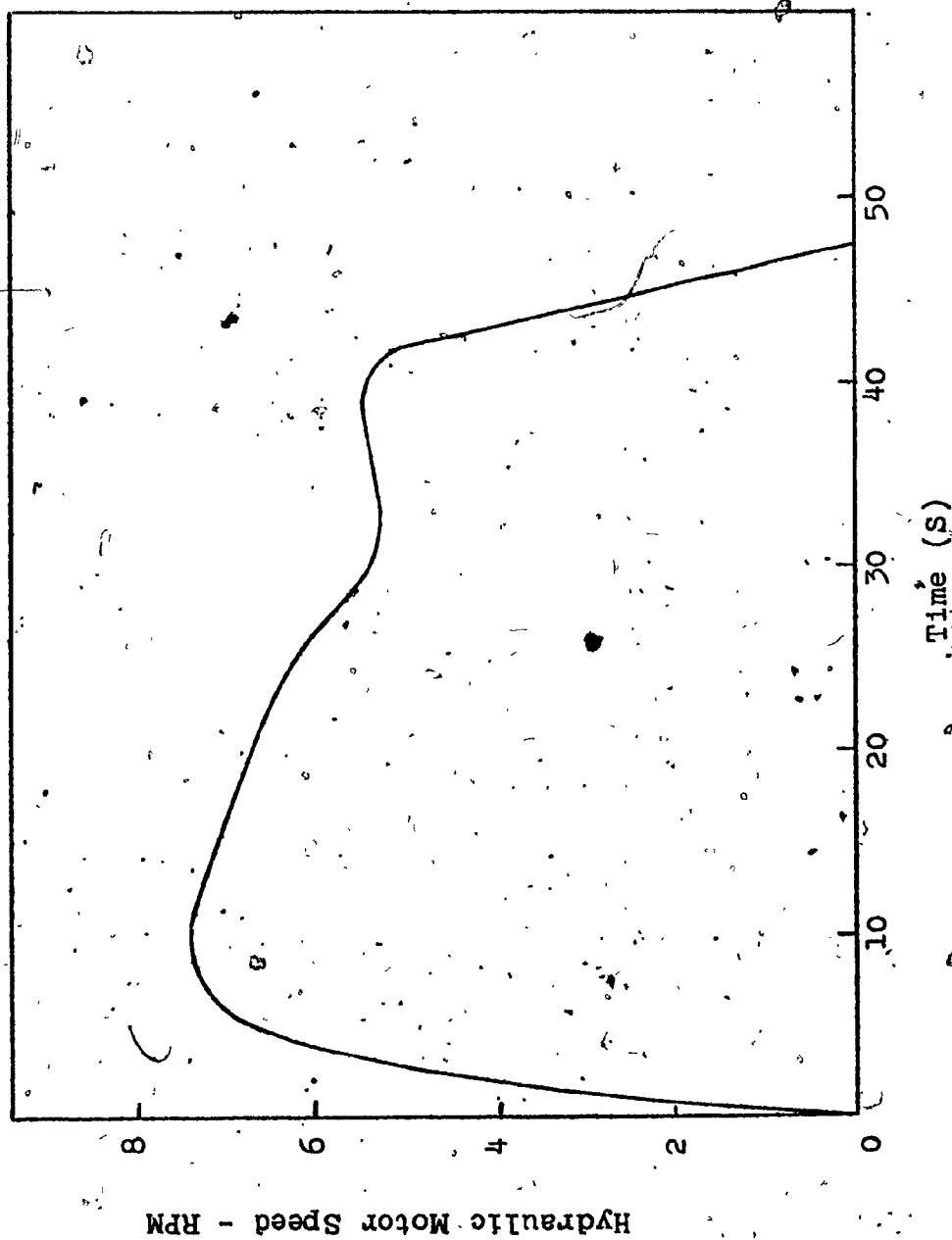


Figure 4.5(a) Time VS Hydraulic Motor Speed - Gate Closing

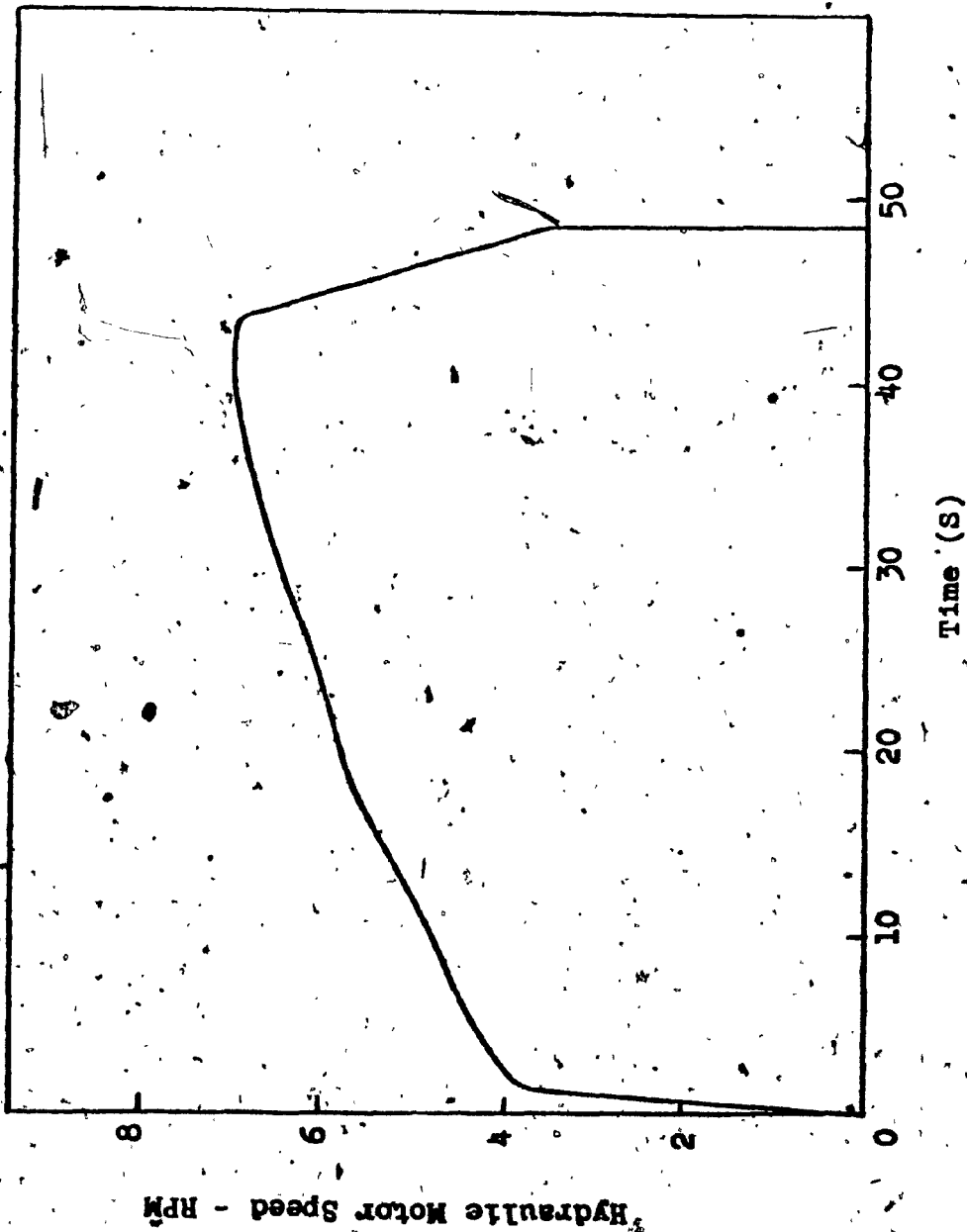


Figure 4.5(b) Time VS Hydraulic Motor Speed RPM - Gate Opening.

Gate Opening Cycle

1. The gate to start opening at maximum system pressure but a speed corresponding to that of the hydraulic motor at 3.5 R.P.M. The reason, as during the closing cycle, is to avoid setting up vibrations of the gate structure.
2. The middle region of the gate opening cycle is to be traversed at maximum possible pressure and speed.
3. Pressure and hence motor torque is again reduced during the final 3° before the fully open gate position.

The hydraulic motor can function as a pump during load reversals created by water surges running in the direction of gate movement. In this mode of operation the system absorbs energy, minimizing any damage which might be caused by the gate slamming against its end position stops. The discharge of the hydraulic motor running in reverse is blocked by a counterbalance valve and passed through a relief valve set at the maximum system pressure.

Although the maximum system pressure has been limited to 14000 KPa, all components were selected for a maximum Pressure of 21000 KPa to allow for possible upgrading of power in the future.

The main components in the circuit are:

1. Hagglunds Hydraulic Motor A8385 L, with a swept volume of 2385 in³/rev. (.00607 m³/rad).

2. Pump No. 1: Vickers Vane Pump 35 V25A - 1C10L-181. This is a fixed displacement pump with a swept volume of 4.8 in³/rev (12.5 x 10⁻⁶ m³/rad) to provide 25 usgpm (0.0269 m³/s) swept volume at 1200 R.P.M.

3. Pump No. 2: Brueninghaus Piston Pump 125 EZ1RP1/R 1120. This is a variable displacement pump with a swept volume 7.6 in³/rev. (19.8 x 10⁻⁶ m³/rad) at the maximum swash angle of 25 degrees.

4. 50 HP, 1800 R.P.M. electric motor for driving both pumps.

The drive control is arranged in such a way that Pump 1 alone provides initial drive; Pump 2 cuts in after the lock gate is in motion. Both pumps drive the gate during most of its displacement. Pump 2 cuts out before completion of gate motion, leaving Pump 1 to complete the final portion of the gate motion.

4.4 Performance Tests of Hydro-Mechanical Gate Drive [6]

4.4.1 General

This portion of the performance tests describes the results of dynamic performance measurements carried out on hydro-mechanical mitre gate drives on St. Lawrence Seaway.

while in operation. The measurements of hydraulic pressures at four points in the drive system, and the angular displacement of the main output shaft of the drive system are made. For each of these five variables, continuous traces were obtained as the gate moved through full operating cycles. The measurements are also made for those cases when ship was using the lock or not.

4.4.2 Measurement Procedure and Recording

The four pressure measurements are made by locating four pressure tapping points in the hydraulic lines as shown in Fig. 1.3. Locations 1 and 2 give the pressure drop across the hydraulic motor when it is driven in either direction or performs as a pump, dissipating the kinetic energy of the gate or the energy of a surge reversing the direction of the normal load on the gate. Locations 3 and 4 allow recording of discharge pressures of both pumps without distortion from other components, also, whether the individual pumps are delivering to the motor or dumping to tank. The difference between locations 3 and 1 or 2 gives the friction loss between the points. 2-Validyne DP22 5000 p.s.i. (35×10^6 Pa) and 2-Validyne DP15TL 3000 p.s.i. (21×10^6 Pa) pressure transducers were inserted in the 4 tapping points. Each was excited by a separate Validyne CD12 transducer indicator with a sensitivity of 2 volts/1000 p.s.i. (7000 K Pa).

The transducer outputs were recorded on a 4 channel Gould-Brush recorder 440-S-1636 with a sensitivity of 0.6 inch/1000 p.s.i. (0.2177 m/1000 K Pa). Angular displacement of the drive shaft (about 8"/0.203 m dia) was measured by a 10 turn rotary potentiometer with a 4-inch (.1016 m) diameter wheel. The potentiometer was held on a magnetic base stand, such that the wheel contacted the drive shaft. The potentiometer was excited by a 6-volt dry battery, and its output displayed on a Gould-Brush 220 recorder such that the full displacement (about 4.5 revolutions) of the shaft caused 8 divisions (about 3.175 cm) per sweep.

4.4.3 Test Results

Thirteen individual tests were carried out with conditions as listed in Table 4.1 with the pump drive speed of 1800 r.p.m. and for total drive shaft rotation of 4.75 revolutions. Fig. 4.6 shows a typical set of such traces for the condition No. 12 specified in Table 4.1.

Fig. 4.7 and 4.8 show mean line diagrams compounded from the readings for gate opening and closing so as to illustrate the system response characteristics. For the gate opening condition as shown in Fig. 4.7, the control valve opens and the gate starts to move 2-3 seconds after the hydraulic supply is started. There is an initial pressure surge of short duration (0.3 s) to system relief valve pressure 13300 KPa. Pump 1 (fixed displacement vane pump, nominal swept displacement of .00227 m³) drives the

RUN	Gate Motion		COMMENT
	Opening	Closing	
1		✓	No Ship
2	✓		No Ship
3		✓	No Ship
4	✓		No Ship
5		✓	Ship moving out east (same way as gate moves)
6	✓		Ship sailing away
7	✓		No Ship
8		✓	No Ship
9	✓		Stopped at 75% open; then closed. No Ship.
10	✓		Stopped at 50% open; the opening completed. No Ship.
11		✓	No Ship
12	✓		No Ship
13		✓	Ship entered, going west

Table 4.1 Lock Gate Operation Pattern

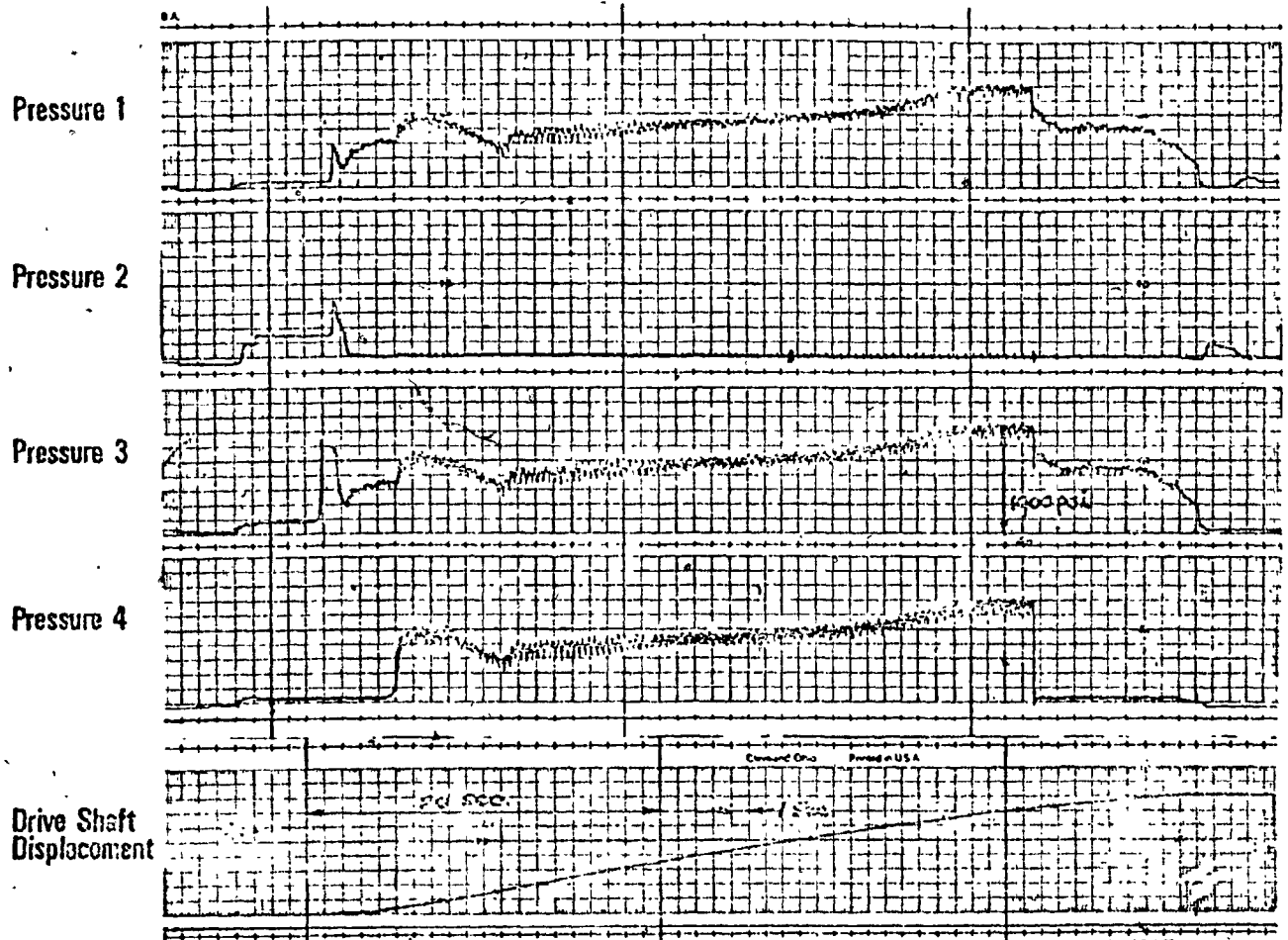


FIGURE 4.6 - GATE CLOSING

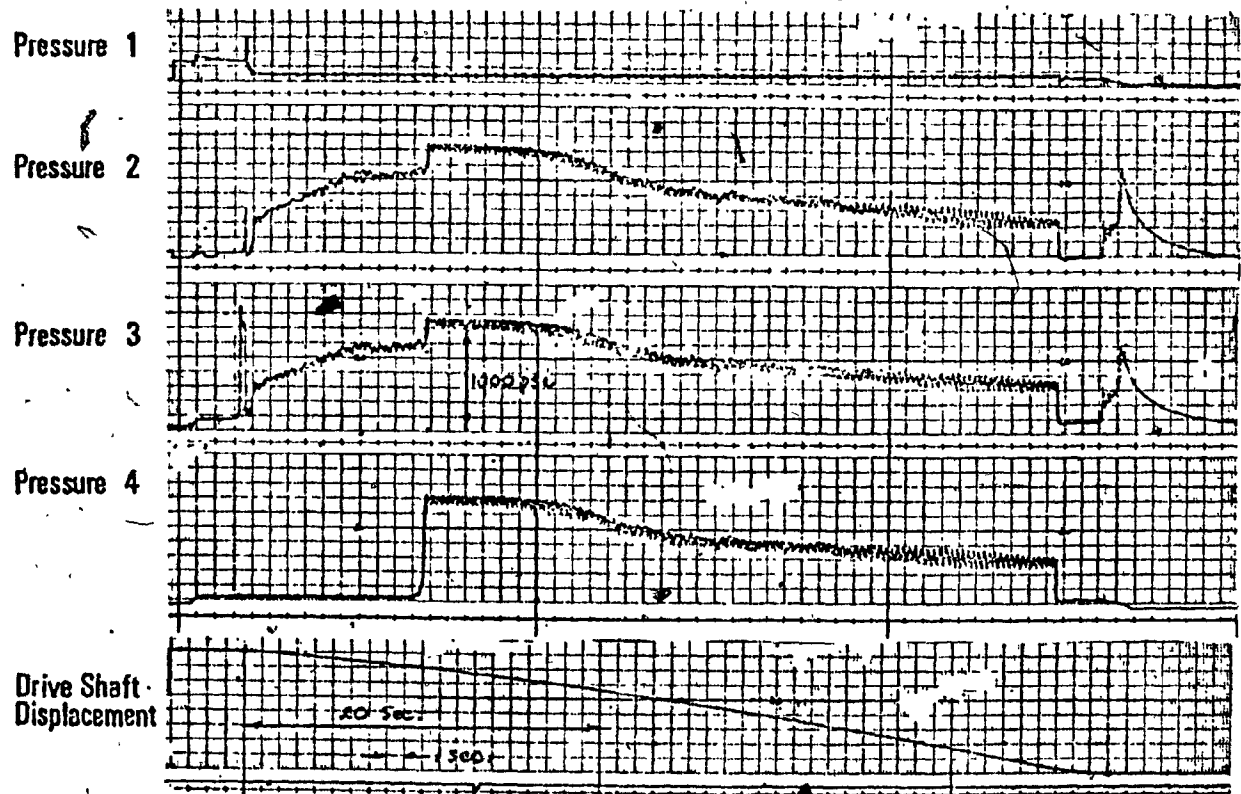


FIGURE 4.6 GATE OPENING

FIGURE 4.6 - ACTUAL TRACES

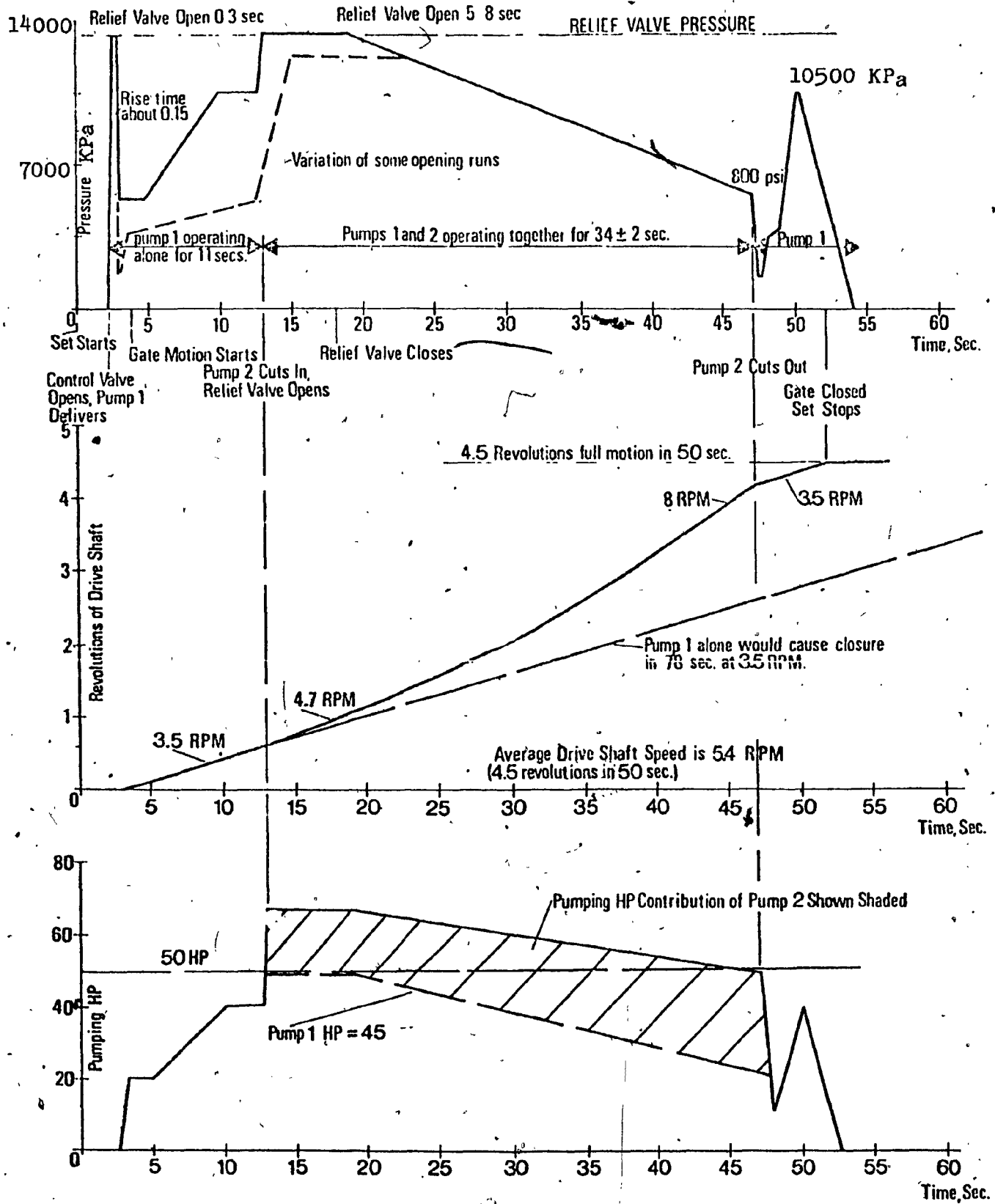


FIGURE 4.7 GATE OPENING CHARACTERISTICS

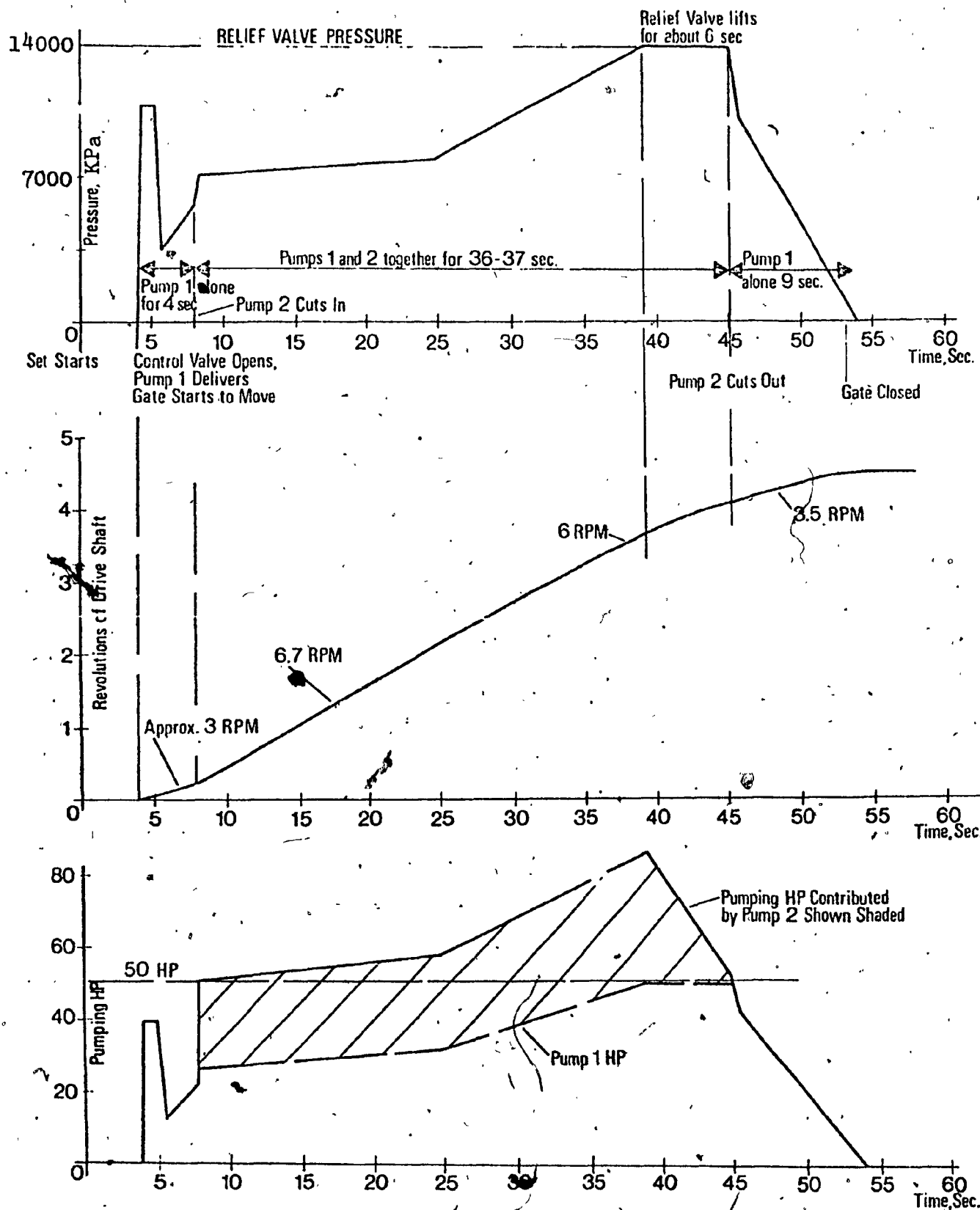


FIGURE 4.8 GATE CLOSING CHARACTERISTICS

gate, with pressure building up to 10500 KPa. After 11 seconds of Pump 1 operation, Pump 2 (variable displacement piston pump, nominal maximum swept displacement of .003785 m³/s, 25° tilt angle) cuts in, forcing system pressure to increase to 13300 KPa limit. This automatically drive shaft speed from 3.5 to 4.7 r.p.m. as shown in Fig. 4.7.(b). The relief valve stays open, dumping some of the pump discharge for about 6 seconds. After this, pressure falls gradually and drive shaft speed increases. This reflects a decreasing resistance to motion offered by the lock gate and its mechanical drive leverage system. After 34 seconds of dual pumping operation, the system pressure decreases to 5600 KPa and drive shaft speed increases to 8 r.p.m. At this stage, Pump 2 cuts out leaving Pump 1 to complete the opening. There is a substantial pressure surge during this latter stage, which lasts approximately 5-6 seconds. For this gate opening operation takes 50 seconds from its initial motion to its full open state. The motion is smooth, though its velocity increases steadily during most of the motion. The initial velocity of the gate when Pump 1 alone operates is 3.5 r.p.m., and if this operation would continue without the operation of Pump 2, then Pump 1 alone would cause gate closure in 78 seconds. Referring to Fig. 4.8 for the gate closing condition, the dead time between set start up and gate movement is approximately 4 seconds. The initial pressure surge is only 10500 KPa which is

considerably small compared to the opening operation.

However the peak pressure is of longer duration (about 1 sec.)

Similar to the opening operation Pump 2 cuts in and the pressure increases to 7000 KPa and remains about constant for

the first 16-17 seconds of dual pump operation, reflecting

a fairly steady gate and mechanism resistance load on the

hydraulic system. After 16 seconds of dual pump operation

the gate is about half open, and the pressure starts to

increase, indicating increasing resisting load. For the last

6 seconds of dual pump operation, the pressure increases

beyond 13300 KPa causing the relief valve to dump some of

the flow and causing shaft speed to reduce. Pump 2 cuts out

after 36 seconds of dual pump operation, and the gate closure

is completed by Pump 1 generating a drive shaft speed of

about 3.5 r.p.m. Maximum shaft speed during closure is

6.7 r.p.m. occurring in the first part of dual pump operation.

The gate is in motion for 50 seconds during closure. The gate

angular velocity varies continuously throughout the closing

cycle and it differs from the opening cycle. Unlike the

opening cycle, the pump pressure falls off smoothly in the

final stage of gate closure.

4.4.4 Corrections to Pump 1 Delivery

An anomaly exists between the rated swept volume of

Pump 1 (36 usgpm at 1800 r.p.m.) and the hydraulic motor speed

measured from the recorded traces (3.5 r.p.m.) when Pump 1

is operating alone.

From Hagglunds information, it is known that the hydraulic motor has a swept volume of $2385 \text{ in}^3/\text{revolution}$. Assuming a volumetric efficiency of 90%, Pump 1 must sweep 2950 in^3 to make the motor turn 1 revolution. Hence for the measured speed of 3.5 r.p.m., Pump 1 must sweep 10,400 in^3/min ; that is 45 usgpm. Therefore, apparent rating (swept volume) of Pump 1 must be 45 usgpm, not 36 usgpm as given in its nominal rating.

Some Possible Explanations:

1. The measured shaft speed values are incorrect.

A thorough checking of 9 separate traces discounts this. There is obviously no wheel slip between potentiometer and drive shaft. There is good consistency between quite separate readings.

The results at the start of Figure 4.7(b) (3.5 r.p.m.) and the end of Figure 4.8(b) (3.5 r.p.m.) are more reliable than the measurement at the start of gate closing as the latter occupied too short a time to take accurate slopes from the traces.

2. Flow additional to that of Pump 1 is provided.

It was thought that Pump 2 might be providing some flow even though it should not be doing so in the initial gate motion stage. A glance at pressure trace 4 shows that Pump 2 cannot be pumping into the motor supply in this stage. If it were, Pump 2 would have to be developing the same pressure as Pump 1.

3. The hydraulic motor swept volume is 20% smaller than expected. This does not seem likely in such a large component.

4. Pump 1 is 24% larger than expected. Pumps of this kind and size are modular in construction. The same casing may contain moving parts of different swept volume ratings. It is not impossible that a pump larger in swept volume than that expected could be delivered. This is not offered as a normal event. It is quite unlikely, but not impossible.

The best explanation was in fact taken to be as the most reasonable.

4.4.5 Hydraulic Power Developed in the Pumps

Figures 4.7(c) and 4.8(c) show the hydraulic power developed by the system during the gate motion. Pumping power is defined as: $\text{Pump Power} = P_a \cdot V_s$ where P_a is the pressure measured at pump delivery; V_s the apparent swept volume of pump(s) per second, derived from actual measured drive shaft speed.

From the power characteristics of the pumps illustrated in Figures 4.7(c) and 4.8(c), the following conclusions can be drawn:

- Maximum pumping power developed is 87 HP, about 45 seconds after start of gate closing. At this point the relief valve flow is undetermined.

-On both opening and closing states, power exceeds the 50 HP continuous rating of the electric motor.

-For gate opening, power overload lasts 32 seconds and reaches 67 HP maximum (for 6 seconds at 13-19 seconds after start).

-For gate closing, power overload lasts 37 seconds and reaches a maximum HP at 45 seconds after start up.

This peak, or something near to it, may last for 6 seconds depending on the action of the relief valve on the power limiting control of Pump 2.

-The power limiting mechanism on Pump 2 (nominally set at 25 HP), appears to be functioning. Figure 4.7(c) (gate opening) shows that Pump 2 power does not exceed about 28 HP and from Figure 4.8(c) (gate closing) the Pump 2 power reaches 36 HP before it is reduced.

-Maximum pumping power of Pump 2 is 67 HP. ($0.062 \times 10^{-6} \text{ m}^3/\text{s}$ and 13300 KPa at 1800 r.p.m., and 25° tilt angle).

4.4.6 Conclusion

1. The drive moves the lock gate in what appears to be a satisfactory manner.

2. The power required is in excess of the primary drive electric motors continuous rating of 50 HP. The motor operates only in an intermittent manner of about 50 seconds duration of which some 35 seconds is at overload.

state. The "gate opening" power reaches 67 HP, while the "gate closing" power reaches 87 HP.

3. The power load is well within the capability of the hydraulic components of the drive.

4. The cutting in and out of Pumps 1 and 2 can be adjusted to reduce the duration of the overload state. The adjustments and tests are described in Appendix C.

4.5 Correlation of Mathematical Model with Prototype Test Results

A statistical correlation between the test and model results will not be attempted because the model assumes a single constant power pump system and the prototype incorporates two pumps of approximately equal power (constant power and fixed delivery). However, certain comparisons can be made between model and pump systems of equal total power, e.g. 50 HP., noting that the prototype is performing in a partially constant power mode during 80 to 85% of total gate travel (Figures 4.7 and 4.8).

The prototype was originally designed with a single constant power pump, but had to be altered due to the pump being unavailable in the desired size and at the required time.

The correlation must be limited to a discussion of trends and ranges of values of the relevant variables.

4.5.1 Hydraulic System Pressure

Figure 4.9 shows a plot of system pressures vs gate operating time for the model and for the corresponding prototype test results.

Comparison of the results is distorted by the difference in pump types and sizes as well as by the constant delivery pump in the prototype having been supplied with a higher than specified output. Moreover, due to the existing gate speed controls of the prototype, the system had to be operated at a slower speed, e.g. the constant delivery pump only, during approximately $1/3$ of the cycle time.

Points which argue in favour of the validity of the model are:

1. When the prototype operates in the partial constant power mode (two pumps), the shape of the pressure vs time curve, and its range of values for the prototype are similar, to a degree, with those for the model. The two-pump operating period of the prototype accounts for over 80% of the gate movement.
2. The relatively long periods of relief valve opening on the prototype cannot be duplicated by the constant power circuit. Pump delivery is cut automatically at a pre-set pressure. Since zero delivery of the model pump was taken as the relief pressure, only the pressure spikes shown in Figure 4.9 can be expected to actuate the relief valve, and they do.

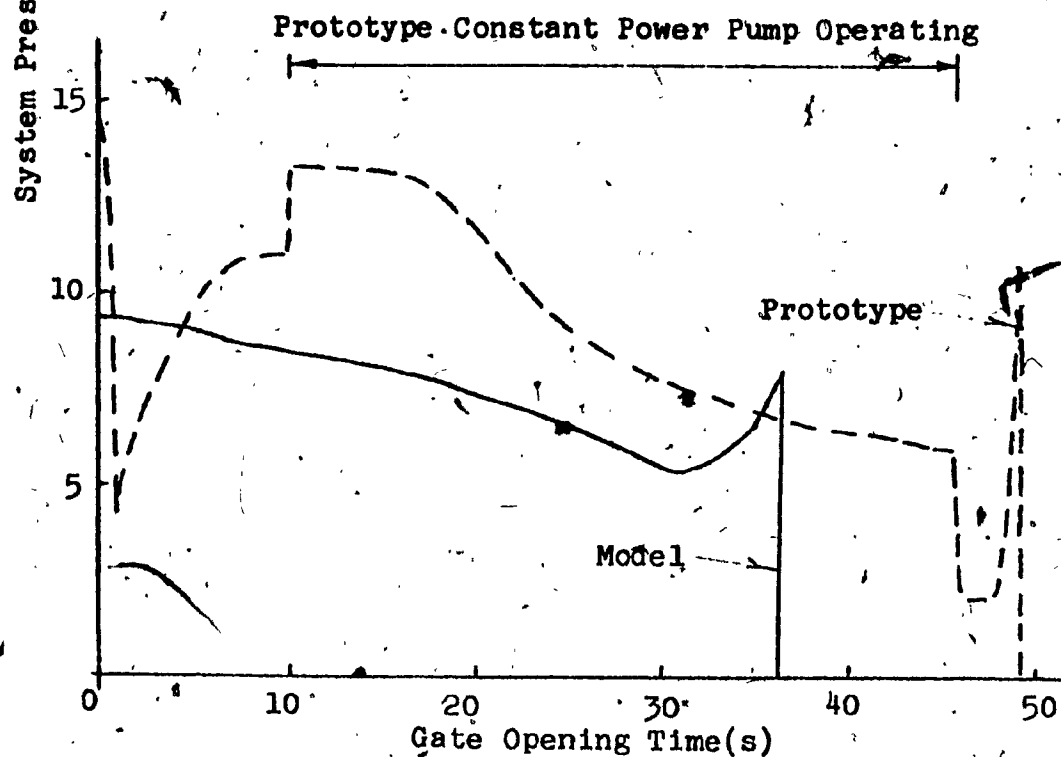
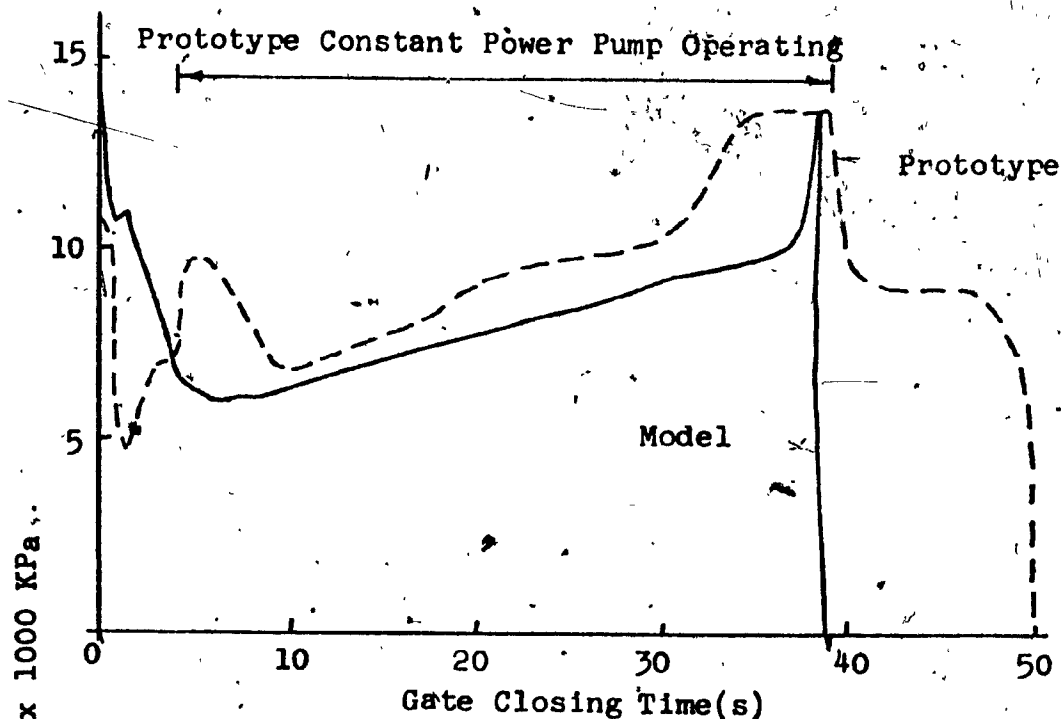


Figure 4.9 Pressure Traces from Prototype and Model

3. Figure 4.9 shows the prototype developing higher pressures than the model, to operate the gate in a time longer than the model. This apparent incongruity can be explained by the work wasted by the prototype through the relief valve and the prototype having a variable flow circuit during most of the gate cycle.

4.5.2 Gate Operating Times

The gate operating time given by the model is 22% and 27% shorter than that of the prototype for gate closing and opening respectively. The differences can be partially accounted for by the deliberate slowing down of the prototype at the beginning and end of each cycle. The slowing down was to prevent gates from impacting their end position stops too hard during single gate operation, where water resistance diminishes. Such a precautionary slowdown can be avoided in the model gate drive with a single variable delivery pump by designing a suitable control circuit. A proposed control circuit is described in Appendix D. It can be concluded from the above comparisons that the constant power system of the model represents the most efficient utilization of power with respect to operating time.

4.5.3 Hydraulic Motor Speed

Table 4.2 compares hydraulic motor speeds. Since the operating times of the model and prototype differ, it was thought more appropriate to compare the speeds at percentages of cycle rather than at a fixed time of operation. Using

TABLE 4.2 HYDRAULIC MOTOR SPEED COMPARISON

% of Gate Cycle Time	GATE CLOSING		GATE OPENING	
	RPM Prototype	RPM Model	RPM Prototype	RPM Model
10	6.7	7.7	3.5	5.5
30	6.5	7.5	4.7	6.0
60	6.0	5.9	8.0	7.8
90	3.5	5.1	3.5	10.5

this comparison method the model and prototype gates are more likely to approximate the same pivoting angle. The speeds are approximate only due to the difficulty of computing the speeds from the prototype test results.

The correlation appears reasonable, in the middle range, where two pumps operate in the prototype. The greater differences at the extremes of the cycles probably reflects the deliberate slowdown of the prototype.

4.5.4 Other Variables

2 Tables 4.3 and 4.4 list a set of values extracted from the computer printout for the model drive of 50 HP. The time values have been selected to show the trend in system pressure and hence in gate torques.

A comparison of the values in the tables with those measured on the prototype drive shows that their ranges and trends are reasonable:

- Gate speeds increase up to mid-point of cycle and thereafter fall as expected.
- Water torques generally follow the pattern of the model test results shown in Figure 5.4.
- The range of values of the various gate torques approximates those measured experimentally on the St. Lawrence Seaway. Also, the gate inertia torque, T_j^g , turns negative during parts of the cycle where deceleration can be expected.

$T_{\text{now}} \text{ (s)}$	$\theta \text{ (rad)}$	$\omega_g \text{ (rad/s)}$	$Q_a \text{ (l/s)}$	$P_a \text{ (Pa)}$ $\times 10^6$	MA	$T_j^g \text{ (N-m)}$ $\times 10^6$	$T_g^g \text{ (N-m)}$ $\times 10^6$	$T_w^g \text{ (N-m)}$ $\times 10^6$	$\omega_m \text{ rad/s}$	$Q_r \text{ (m}^3/\text{s)}$
3.6	1.80	.02	3.50	9.1	24.4	.0183	1.242	1.136	.576	0
8	1.68	.031	3.77	8.54	20.0	.0106	.948	.851	.620	0
11	1.58	.0337	3.83	8.41	18.7	.0161	.876	.773	.631	0
14	1.48	.0359	3.96	8.17	18.6	.0107	.823	.725	.653	0
20	1.25	.0405	4.55	7.22	18.5	.0119	.741	.642	.750	0
26	1.00	.0403	5.22	6.38	21.3	-.0092	.749	.672	.859	0
31	.806	.0386	6.59	5.13	28.1	.0019	.796	.707	1.085	0
34	.696	.0317	5.77	5.81	30.0	-.0468	.945	.905	.951	0
36	.637	.0225	4.09	7.96	30.0	-.0677	1.274	1.254	.674	0

Table 4.3. Simulated Performance Variables for Gate Opening, 50 HP Drive

T_{row} (s)	T_j^E (N-m) $\times 10^6$	T_g (N-m) $\times 10^6$	T_w^E (N-m) $\times 10^6$	ω_m (rad/s)	Q_r (m ³ /s)	θ (rad)	ω_g (rad/s)	Q_g (m ³ /s)	P_a (Pa) $\times 10^6$	MA
.03	1.056	1.148	.0051	.344	.00013	.634	.0115	2.09	14.13	30.0
1.5	.030	1.768	1.650	.4768	0	.661	.0159	2.89	10.65	30.0
4.1	.023	1.110	1.000	.8244	0	.716	.0272	4.95	6.669	30.0
6	.000	.997	.891	.9233	0	.774	.0308	5.60	5.967	30.0
10	.000	.826	.735	.868	0	.911	.0368	5.27	6.326	23.4
20	.000	.790	.707	.687	0	1.288	.0375	4.17	7.815	18.3
30	-.019	.975	.908	.566	0	1.632	.0294	3.14	9.237	19.3
37	-.082	1.315	1.310	.516	0	1.810	.0206	3.13	10.020	25.0
38	-1.023	1.120	2.054	.326	.00012	1.833	.0120	2.00	14.69	27.3

Table 4.4 Simulated Performance Variables for Gate Closing, 50 HP Drive

CHAPTER V

OPTIMIZATION

5.1 General

The cost of any gate drives in navigation locks depends directly on its horse power requirement which in turn determines the operating time of the gates. Since the operating time has a direct relationship with the time a vessel spends in a lock, and hence with the vessel's utilization, it is desirable to establish the drive's power at which net savings in shipping goods through the Seaway are maximized. Such a cost optimization is presented in this chapter for a hydro-mechanical mitre gate drive simulated in Chapter III.

5.2 Assumptions

1. It will be assumed that the users of the St. Lawrence Seaway and those benefiting from it finance its operation entirely through tolls and indirect taxation, i.e. the moneys spent are by and for the benefit of the users. This ideal is at best only approximated.
2. The life of the gate drives after modification will be 15 years.
3. Interest rates prevailing in the above period will average 12%.

4. Traffic patterns through the Seaway will be maintained, i.e. 7000 vessels transiting per year, with the average cost of operating a vessel \$5000/day.

5. Vessels using the Seaway are fully utilized. (have no idle time).

5.3 Utilization Costs

The benefit obtained by reducing the operating times of the gates $\$u^t$, can be written as

$$\$u^t = N_s \cdot \$u \cdot T_s \quad (5.1)$$

where N_s is the number of ships passing the gates annually, $\$u$ the monetary value to vessel owners of each second of added vessel utilization time, and T_s is the number of seconds by which the gate operating time is reduced.

The Present Value Method [16] is used to calculate the cost saving over the next 15 years

$$\begin{aligned} \$_{pv} &= 6.81 \times 405.09 T_s \\ &= 2759 T_s \quad (\$) \end{aligned} \quad (5.2)$$

The computer program in Appendix B is used to calculate a range of operation times corresponding to a gate drive power range of 10 to 50 HP, in steps of 5 HP and is presented in Table 5.1. The average of an opening and closing time of the simulated hydro-mechanical drive subtracted from the average operating time of the electro-mechanical drive mechanism (72 seconds), gives the average operation time saving due to the modification. The values

HP	Time For Gate Opening (s)	Time For Gate Closing (s)	Average Time For a Gate Cycle (s)
10	68.28	73.25	69.77
15	56.43	62.72	59.57
20	50.52	56.34	53.43
25	46.36	51.94	49.15
30	43.29	49.44	46.37
35	41.07	46.20	43.64
40	39.30	43.40	41.35
45	37.55	41.23	39.39
50	36.22	39.09	37.66

Table 5.1 Gate Operating Times

of T_s thus obtained and substituted into Equation (5.2) give values of $\$_{pv}$. These values of $\$_{pv}$ vs HP are shown plotted in Figure 5.1.

5.4 Cost of Gate Drive Modification

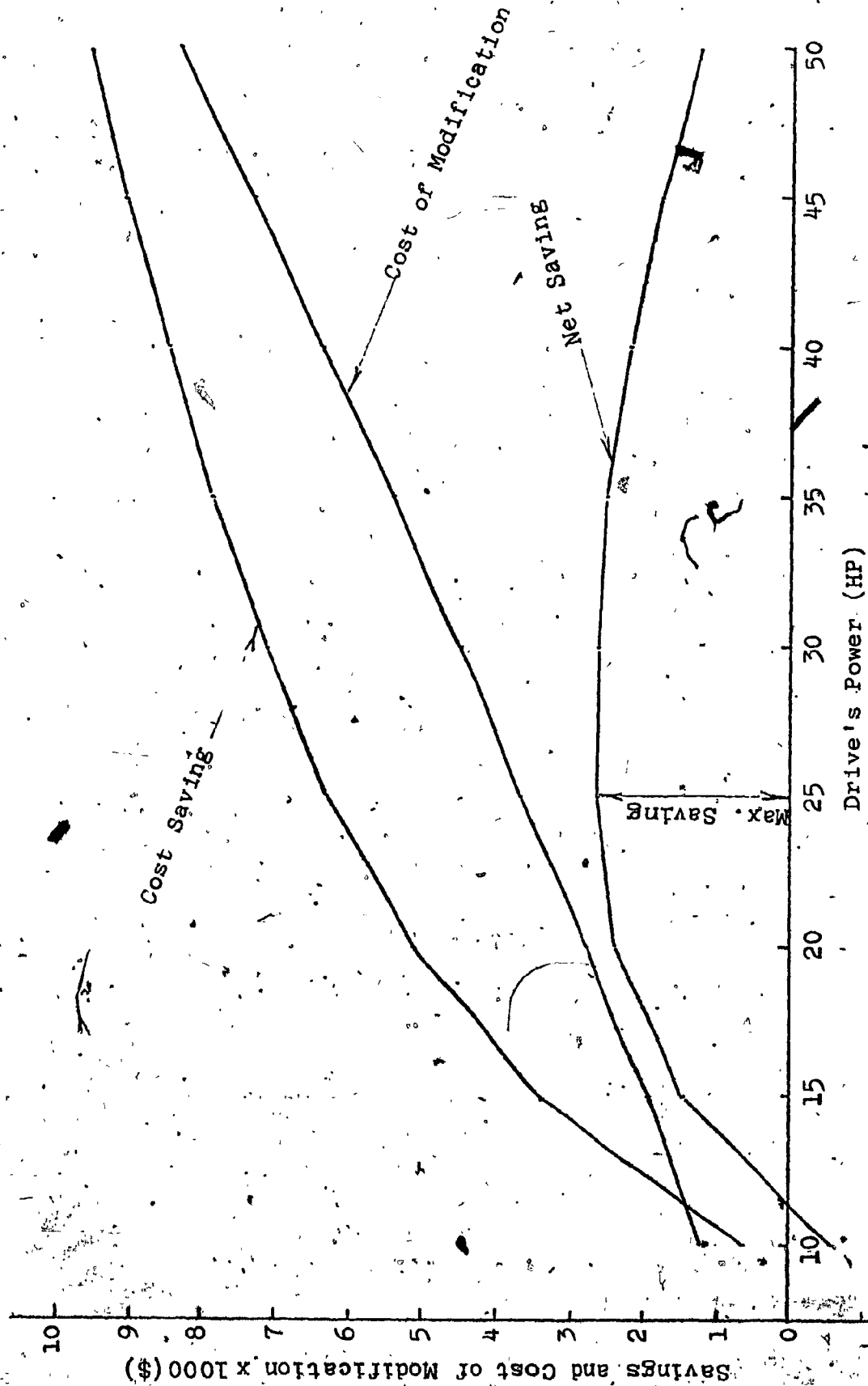
The cost of modifying a 50 HP electro-mechanical drive to a hydro-mechanical drive of identical power is known to be \$83,000 from industrial quotations. To estimate the cost of drives of different power, an empirical rule used by estimators for hydraulic assemblies at equal operating pressures is employed. This empirical formula is given by the relationship

$$\frac{\text{The cost of Drive 1}}{\text{The cost of Drive 2}} = \left(\frac{\text{HP of Drive 1}}{\text{HP of Drive 2}} \right)^{1.2} \quad (5.3)$$

Using the cost estimate of a hydro-mechanical drive of 50 HP and the relationship given above, the cost estimate for a range of drive powers are calculated and plotted in Figure 5.1.

5.5 Optimum Power

The difference between the total cost saving due to shorter gate operating time in a hydro-mechanical drive and the cost of the gate drive itself gives the overall cost saving. This difference represents the benefit due to the conversion. A plot of this overall cost saving for a range of power is shown in Figure 5.1. From this plot it can be observed that the maximum benefit occurs with a drive of



Figures 5.1. Cost Optimization

<u>Surge Time Lag(s)</u>	<u>Gate Closing Time(s)</u>
0	85.35
18	75.81
36	64.44
54	53.43
72	44.99
90	39.93
108	37.88
126	38.65
144	47.05
167	60.8
180	85.35

Table 5.2 Effect of Water Surging

approximately 25 HP with a slight edge over the cost saving between drives ranging from 20 to 35 HP.

The mathematical model used for calculating the gate operating times used in the optimization did not include the effect of water surging in the lock. The effect of surges which occur infrequently can be discounted in the power optimization. However, the surges influence the maximum range of gate operation times, which is of interest to lock operators. The influence of surges has been investigated for the gate drive at optimum power and is presented in Section 5.6.

5.6 Effect of Water Surging

The computer program listings in Appendix B include the calculation of the water surge effect formulated by Equation (3.6.20). Table 5.2 shows the times to close mitre gates, with a 25 HP hydro-mechanical drive, and the corresponding times by which the start of a surge cycle lags behind the start of gate closing.

Examination of Tables 5.1 and 5.2 shows closing times for the 25 HP drive to be:

- 52 seconds without water surging.
- 85 seconds as the maximum time occurring with the surge in phase with the start of closing.
- 38 seconds as the minimum, occurring at a surge phase lag of 108 seconds. In this case the surge acts in the direction of gate closing.

CHAPTER VI

CONCLUSIONS

6.1 General

In this chapter the results obtained from the digital simulation of the mathematical model and prototype experimental tests will be discussed. Based on the results, conclusions will be drawn, and further applications of the mathematical model and of the hydraulic circuit tested in the prototype will be proposed. Future work will be suggested to augment that described herein.

6.2 Discussion of Mathematical Model and Prototype Results

Examination of computer printouts for model gate drives in the 10 to 50 HP range shows the dominant role of the water resistance. In the 50 HP drive (shortest gate operating cycle), the inertia torque is negligible during the opening cycle and is only significant in the first and last two seconds of the closing cycle (Table 4.4). Friction torque averages approximately 10% of the total torque on the gate and the remainder is accounted by the water resistance. In the lower HP range, inertia torques become even less significant and the constant friction torque takes on added importance.

The preponderance of the water resistance explains why the original cycle time estimates for the prototype, obtained by assuming the resistance as the sole load on the gate, were reasonably accurate.

The better operating times given by the model when compared with the prototype imply an advantage of pure constant power systems over constant flow systems. Since some of the time disadvantage of the prototype can be attributed to the rather cumbersome gate speed controls employed, controls of the type described in Appendix D appear desirable. At the optimum power of 25 HP, the gate speeds at start and termination of cycle are acceptable at the normal operating conditions, and the control would only be employed as a precautionary measure, e.g. to slow the gate down in case of a single gate operation.

The need for better controls has been demonstrated in prototype tests which have been carried out to reduce the operating time through better timing of cutting in and out of the constant power pumps. The additional tests are described in Appendix G.

The test results obtained by the U.S. Army Engineer Waterways Experiment Station for gate water resistances, Figure 3.4, contain sharp spikes. The time interval ΔT_{now} now in the computer solution must be kept very small in the area of these spikes to avoid undue fluctuations or overcalculations in other variables. The same approach

applies to other pressure spikes, e.g. the working of relief valves.

6.3 Applications

The results of the simulation and actual tests show the constant power, hydro-mechanical machinery to be superior to the electro-mechanical drive. Existing 20 HP electro-mechanical drives on the St. Lawrence Seaway give an operating time of 72 seconds while working part of the cycle at higher than nominal power. The simulation shows that a 20 HP constant power drive operating the gate, has an average operating time of only 53.43 seconds (opening cycle = 50.52 seconds; closing cycle = 56.34). Also the hydro-mechanical drives are less expensive [5] when installed in new navigation locks.

The results of the simulation indicate that the inertia torques on the gate are negligible except for two momentary high values at the beginning and end of the gate closing cycles. Based on experience with the 50 HP prototype, the torque peaks which correspond to pressure peaks (Table 4.4), will not disturb the smooth operation of the gates. The assumed hydraulic motor size gives system pressures below 10,000 KPa, except during the two pressure peaks referred to.

Generally, the principle of the constant power drive and the simulation described herein can be usefully applied to all gate drives. This gate drive appears to be particularly useful where the resisting load changes relatively fast and in an irregular pattern. The self-governing properties of the drive will ensure that close to optimum operating times are obtained with a given power input. The simulation should be useful in estimating the operating times, pressures and flows for new drives or those to be modified from electro-mechanical. Knowledge of these variables is essential in rational sizing of drive components.

6.4 Future Work

1. Future work should involve a complete validation of the model by tests. The ideal test program would involve changing the hydraulic circuit of the 50 HP prototype drive to allow operation on the constant power pump only while dumping the constant delivery pump to tank.
2. The constant power hydraulic circuit can be applied to gates using cylinders instead of motors as actuators.
3. The simulation of the 25 HP drive gives hydraulic pressures not exceeding 10,000 KPa. Since pressures 50% higher are acceptable in the type of system considered, an optimization of motor size is indicated.

REFERENCES

1. The St. Lawrence Seaway Authority, Publicity Pamphlet, 1976.
2. Amster, M.N., Hydraulic Investigation of Mitre Gate Operation, The Panama Canal Special Engineering Division, 1942.
3. Dehnert, H., Schleusen Und Heblenwerke, Springer-Verlag, 1954.
4. The St. Lawrence Seaway Authority, Proposals for 110 foot Locks for Welland Canal, 1968.
5. Corps of Engineers, Supp. 1 to Lower Granite Design Memo 20 - Mitre Gate Operating Machinery, U.S. Army Engineer District, Walla Walla.
6. Dransfield, P., Desjardins, Y., and Elliott, J., Concordia University Fluid Control Centre, Report no. FCC - 0026, 1975.
7. Dransfield, P., Lecture Notes, Concordia University, 1975.
8. Dransfield, P., "Power Bond Graphs", Machine Design, October 6, 1975, pp. 134-138.
9. Liou, M., Surge Study Côte Ste-Catherine Lock, E1-009, The St. Lawrence Seaway Authority, November 1969.
10. Lejeune, A.G., Non-Steady Two-Dimensional Flow About a Uniformly Rotating Plate, Journal of Hydraulic Research, 12 (1974) no. 1, pp. 66-81.
11. Grace, J.L., Jr., Murphy, T.E., Brown, F.R., Operating Forces on Mitre-Type Lock Gates, U.S. Army Engineer Waterways Experiment Station, Vicksburg, 1964.
12. The St. Lawrence Seaway Authority, Memo of Accident Investigation Committee on Misoperation of Dumping Valve, Lock 2, 1972.
13. Canadian Standards Association, Movable Bridges, Standard S20, CSA, 1960.
14. Lewitt, E.H., Hydraulics, 9th ed., London Pitman, 1955.
15. Ippen, H.T. Estuary and Coastline Hydrodynamics, New York, McGraw Hill Book Company, 1966.
16. Bierman, H. Hr., The Capital Budgeting Decision, 2nd ed., The McMillan Company, New York, 1968.

APPENDIX A

POWER BOND GRAPHS

Preface

Power Bond graphs owe their development to D. Karnapp and R. Rosenberg. P. Dransfield of Monash University, Australia has done considerable work in applying the graphs to hydraulic systems and the following is a brief summary of this graph. [7, 8].

Purpose of Power Bond Graphs

The graphs are an alternative technique of dynamic response evaluations to transfer functions, block diagrams and signal flow graphs. They are particularly suitable in hydraulic circuit analysis and offer the following advantages:

- Straightforward dynamic modelling suitable for computer solution.
- Recognition of nonlinearities such as friction, orifice flow, and valve lap.
- Ability to re-use authenticated models of common hardware items.
- Ability to construct the system model directly from a layout of the hardware.
- Quick modification of the model when hardware is added, deleted, or changed.

Power Bond Graph Description

To use the power bond graphs, a set of definitions and symbols must be defined. Table A1 summarizes such a description and a brief explanation of this is given as follows:

A power bond is a line used to show each path in which power flows in the system. Each line on the graph is a power bond. Effort, E , is the general term for a potential variable. Flow, Q , is the term for a flow variable. On each power bond there will be an effort and a flow variable to describe the power flowing in the bond.

A source is a power "variable" that is constant, or assumed to be constant for analysis purposes. Source of effort is denoted SE.

A transformer describes power conversion. For example, in cylinder, hydraulic power is transformed to mechanical power: Here, input effort (pressure) transforms to output effort (force) and input flow (oil flow) transforms to output flow (piston velocity). This transformation has the symbol TF. Effort transformed to flow or flow transformed to effort is gyration and is denoted by GY.

Resistive power dissipation, is denoted by a power bond leading to an R.

Capacitive power storage is denoted by a bond leading to a C.


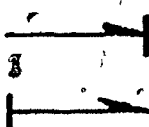
Term	Symbol	As Used in PBG	Meaning
Power Bond	—	$\frac{E}{Q}$	Power flow in the bond equals the product of E and Q. Effort means potential. Flow means flowrate.
Effort	E		
Flow	Q		
Source	SE	$\frac{SE}{Q}$	Effort is constant.
	SQ	$\frac{E}{SQ}$	Flow is constant.
Transformer	TF	$\frac{E_1}{Q_1} \text{ TF } \frac{E_2}{Q_2}$	E_1 transforms to E_2 , Q_1 transforms to Q_2 so that $E_1 Q_1 = E_2 Q_2$
	GY	$\frac{E_1}{Q_1} \text{ GY } \frac{E_2}{Q_2}$	E_1 transforms to Q_2 , Q_1 transforms to E_2 so that $E_1 Q_1 = E_2 Q_2$
Resistive Effect	R	—R	Recognizes a resistive effect.
Capacitive Effect	C	—C	Recognizes a capacitive effect.
Inertive Effect	I	—I	Recognizes an inertia.
0-Junction	0	$\frac{E}{Q_1} \text{ 0 } \frac{E}{Q_2}$	Algebraic summing of flow variables at same E. $Q_1 + Q_2 + Q_3 = 0$
1-Junction	1	$\frac{E_1}{Q} \text{ 1 } \frac{E_2}{Q}$	Algebraic summing of effort variables at same Q. $E_1 + E_2 + E_3 = 0$
Power Flow Direction	(Half arrow on one end of each bond)		Shows direction of power flow in each bond. Easily decided for main power flow sequence. Power flows into R, C, I, elements (a convention). Gives sign convention for equations to be formed for junctions.
Causality	(Short bar across one end of each power bond)		Shows which of the 2 variables on a bond is cause and which is effect. Decides how R, C, I, equations are to be arranged. Only 1 causal bar can be at an 0-junction. Only 1 bond can be at a 1-junction without a causal bar. C elements have causal bar away from the C end. I bonds have causal bar at the I end. Effort is directed at the causal bar, flow away from it.

Table A1. Basic Terms and Symbols for Power Bond Graphs

Inertial power storage is denoted by a bond leading to an I.

Resistive, capacitive, and inertial effects determine dynamic response of the system, and the form of the dynamic equations that make up the system model.

Like signal flow diagrams, power bond graphs require summing junctions at which variables are added algebraically. Because bond graphs are dual signal diagrams, they require two distinct kinds of summing junction. Flow variables are added at a 0-junction, and effort (or potential) variables are added at a 1-junction.

The 0-junction can be understood by thinking of a tee in a hydraulic line; the algebraic sum of the flow rates at the tee is zero and pressure is the same in each branch of the tee. The 1-junction is exemplified by a rigid piston-mass-load combination. Frictional force must be subtracted from hydraulic force on the piston to give the net force accelerating the mass, but velocity is the same for each component.

The 12 definitions discussed are sufficient to form a power bond graph structure. Further defining 2 symbols - a half arrow for power flow direction, and a transverse bar for causal decisions - make equations easy to write from the graph.

A half arrow head on each bond indicates the assumed

direction of power flow in the bond, and dictates the signs of the summing equations to be written for each O and 1-junction. Power is shown flowing into each R, C, and I element. Also, power is shown flowing from power source to driven load.

Establishing causality is complex. It is the most unique aspect of the technique. It is an organizing and checking step intended to put the vital R, C, I relationships into forms suitable for computer solution. The causal bar shows which of the two power state variables on the bond is to be expressed in terms of the other, through an R, C, or I function. For example, the bond Fig. A2(a) indicates that the equation may be of either form

$$F_m = I_m(X_n)$$

or,

$$X_a = I_m(F_m)$$

where $I_m(Z)$ denotes an inertia function of Z . Placing the causal bar at one end of the I_m bond indicates a decision as to which of these arrangements is to be prepared. If the causal bar is at the I_m end, as in Figure A2(b), then the expression is to be prepared as

$$X_a = M_m(F_m)$$

With causal bar at the other end of the bond, the equation would express net force, F_m , as a function of load velocity X_a .

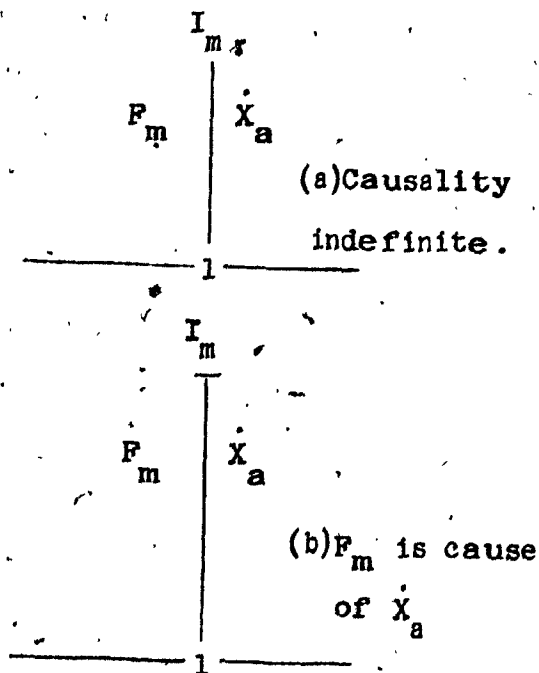


Figure A2 - 1-junctions:
 (a) without causality bar,
 (b) with causality bar. The bar at the I_m end of the bond indicates that force F_m acting on an inertial load I_m is the cause of velocity \dot{X}_a .

Because computers excel at integration, rate equations should be written in integral form. For this reason, causal bars on I bonds are always placed at the I end. This requires Newton's Law to be expressed as

$$\dot{X}_a = (1/I_m) \int P_m dt + \dot{X}_a(0)$$

For similar reasons, the causal bar on a C power bond is always placed away from the C end of the bond, indicating that the functional equation is to be sought in the form of effort as a function of flow:

$$P_a = P_a(Q_c)$$

If a linear capacitance relationship is used,

$$P_a = (1/C_a) \int Q_c dt + P_a(0)$$

I and C elements are given preferred causalities to provide integral equations. Other rules in assigning causality to power bond graphs are:

1. A Q-junction can have only one causal bar at the junction. This means there can be only one effort variable at a Q-junction, just like there can be only one pressure at a tee.
2. A I-junction can have only one power bond without a causal bar at the junction. This means that there can be only one flow variable at a I-junction, which is like saying that rigidly coupled piston-load mass components must have the same velocity.

With these rules, causal assignment on power bond graphs is straightforward. If ambiguity remains in some bonds, one must evaluate the cause-effect nature of the variables on those bonds. The resolution of causal conflicts gives a check to the validity of the proposed model.

Graphs

The power bond graphs are derived from basic circuit diagrams, consider the simple hydraulic system of Fig. A3(a). Assume that constant pressure is supplied to the valve, that hydraulic supply lines have no pressure losses, and that return-line effects are negligible.

Fig. A3(b) shows the power-bond-graph structures proposed for each of the three major components. For the control valve, resistance R_v absorbs power. SP. Q_s is the power supplied by the valve to the component to be connected to it. R_v controls Q_s , and R_v is a function of valve spool displacement X_1 .

For the cylinder, power is supplied in the form $P_a Q_a$. Some power is lost due to the compressibility effect C_a . It is accounted for at a 0-junction, as it is flow that is lost. This leaves $P_a Q_a$ flowing from the junction, where $Q_a = Q_s - Q_c$. P_a is transformed by ram area A to force F_a on the ram, while flowrate Q_a is transformed to velocity \dot{X}_a . For the load mass I_m , use is made of the 1-junction to subtract the friction force F_1 from the pressure force F_a to leave net force F_m acting on the mass I_m . The load will receive power in the form $F_a \dot{X}_a$.

The system graph is formed by coupling of the three graphs, Fig. A3(c). Using the conventions that power flows into R, C, and I elements, and flows from source to load, the half arrows in Figure A3(d) can be added.

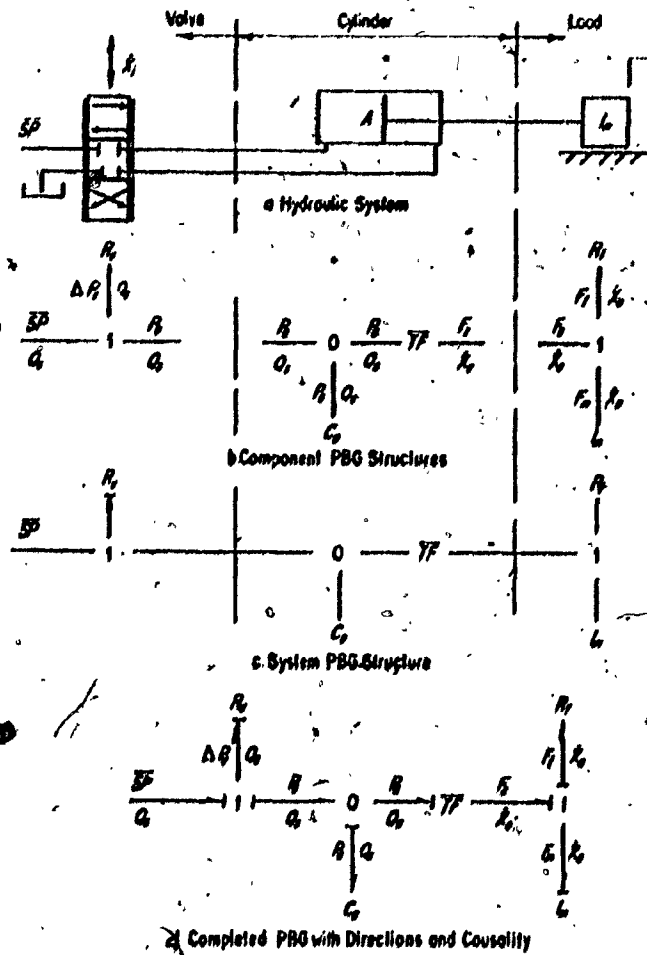


Figure A3. Simple Hydraulic System

Most of the causal assignments fall into place with the following conventions:

- An I bond must have its causal bar against I.
- A C bond must have its causal bar away from the C.
- A O-junction can have only one causal bar against it.
- A 1-junction must have causal bars against it on all bonds except one.

In the example, the only doubtful case of causal assignment shows up at the 1-junction, which has both R_v and SP bonds. It is physically appropriate to think of flow through the valve as a function of pressure drop, so the causal bar of the R_v bond must be at the R_v end. Alternatively, supply pressure is a cause, as it has been assumed constant, so the causal bar must be in the power flow direction, against the 1-junction. In that case, the R_v bond must still have its causal bar at the R_v end. Common sense resolves the doubt.

Equations

From the power bond graph, dynamic equations for the system are developed with a four-part process. First, describe each source. Next, write an equation relating the power variables on each R, C, and I bond, using causality. Then write equations describing each TF and OY action.

Fourth, write an expression for the summation at each 0 and 1-junction, using power flow arrowheads to decide the signs of the terms. Arrange terms so that the left side of each equation is a variable not appearing as the object of an R, C, I, TF, or GY equation.

This procedure gives the set of power state equations, one for each power bond variable. Auxiliary equations can be added to describe any undefined coefficients or terms used in the power state equations, or to describe any desired variables definable from the power state variables.

For the system of Figure A3, from Figure A3(d),

Source: $SP = \text{constant}$ (assumed)

$$R_V: Q_S = R_V (\Delta P_V) = KX_1 \text{sgn} (\Delta P_V) \Delta P^{\frac{1}{2}}$$

where K is flow coefficient

$$C_A: P_A = P_A(0) + (1/C_A) \int Q_A dt$$

$$R_f: F_f = R_f(\dot{X}_A) \quad (R_f \text{ to be specified})$$

$$I_m: \dot{X}_A = \dot{X}_A(0) + (1/I_m) \int F_m dt$$

$$TF: P_A = P_A A$$

$$Q_A = \dot{X}_A A$$

$$1\text{-Junction: } P_V = SP - P_A$$

$$0\text{-Junction: } Q_O = Q_S - Q_A$$

$$1\text{-Junction: } F_m = F_A - F_f$$

Auxiliary: $X_1 = (\text{input to be specified})$

$$X_m = \int \dot{X}_m dt \quad (\text{desirable response variable})$$

APPENDIX B

COMPUTER PROGRAM LISTINGS

IDENT NAME

(0001)

REAL NA

(0002)

COMPLEX PT(17,2),P=DELTA,T=TDON,TRG,IG,IJF,NG,PT,PSI,NA,IFG,THETA,

IRM,VV,OA,PA,GI,GR,DI,HP

(0003)

EO 15 U=1,17

(0004)

EO 15 L=1,2

(0005)

GEAR(5,2)PTI(1,1) 0

(0006)

2 FORMAT(F10.4)

(0007)

-15 CONTINUE

(0008)

DO 16 K=10,5015

(0009)

HP=K

(0010)

CALL INITIA

(0011)

17 CONTINUE

(0012)

DELTA = 0.20

(0013)

IF(THETA.GT.1.805)DELTA=0.91

(0015)

IND = IND + DELTA

(0016)

CALL PTVALU

0.0000000000

0.0000000000

0.0000000000

0.0000000000

0.0000000000

0.0000000000

0.0000000000

0.0000000000

0.0000000000

0.0000000000

0.0000000000

0.0000000000

0.0000000000

100-100000-100000

100-100000-100000

100-100000-100000

THEY WERE NOT IN THE HOUSE AT THE TIME OF THE SHOOTING.

THEY WERE NOT IN THE HOUSE AT THE TIME OF THE SHOOTING.

THEY WERE NOT IN THE HOUSE AT THE TIME OF THE SHOOTING.

```

SUM(FUNCS:CV:IP)=E10.43 * OSI*(E10.44-PA)+
SUM(FUNCS:CV:IP)=E10.43 * OSI*(E10.44-PA)+

```

[illegible]

CHENG, Y. T. and CHAN, S. Y. 1981, *Plasma*, Vol. 9, Pt. 1, 171-183.

1-230-30-1111

FROM THE DELTA, THRU THE TOWNS, PT. PSI, NA, IFG, THETA,

TO THE TOWNS, PT. PSI, NA, IFG, THETA,

TO THE TOWNS, PT. PSI, NA, IFG, THETA,

TO THE TOWNS, PT. PSI, NA, IFG, THETA,

TO THE TOWNS, PT. PSI, NA, IFG, THETA,

TO THE TOWNS, PT. PSI, NA, IFG, THETA,

TO THE TOWNS, PT. PSI, NA, IFG, THETA,

TO THE TOWNS, PT. PSI, NA, IFG, THETA,

RECEIVED 11/17/52 1:40 PM DELTA 1404 1315 16 131F 16 PY PSI MA TFG THETA

131F 16 PY PSI MA TFG THETA

131F 16 PY PSI MA TFG THETA

131F 16 PY PSI MA TFG THETA

131F 16 PY PSI MA TFG THETA

131F 16 PY PSI MA TFG THETA

131F 16 PY PSI MA TFG THETA

131F 16 PY PSI MA TFG THETA

131F 16 PY PSI MA TFG THETA

131F 16 PY PSI MA TFG THETA

131F 16 PY PSI MA TFG THETA

131F 16 PY PSI MA TFG THETA

131F 16 PY PSI MA TFG THETA

131F 16 PY PSI MA TFG THETA

131F 16 PY PSI MA TFG THETA

Room 6002

-111-

00511

14 CONTINUE

STOP

END

MEMORIS COMPILED (75/121)

5:59 P.M.

RELEASE NUMBER: ASR 3.6

ELAPSED TIME 43 SECS

0 FLAGS 0 ERRORS

59 CARDS AT 82 C.P.M.

592 YENDCHARIS = 76

21

CONTINUED FROM PAGE 7: HP, DEI TA; TNDV; TUG; IG, TJF, WG, PT, PSI, NA, TFG, THETA,

THE

22

1990

1992

THE

1983

THE

THE

1991

1990

70-61128(1)A-1

THE

1990

(0017)	TWG = 0.651EB*PI*WG**2.0	C
(0018)	IS = 0.00514*PSI*NA	C
(0019)	TWIG=1436085.0*SIN(0.0343*(TNOW+I))*SIN(THETA-0.634)	C
(0020)	TJF=IG-TWG-TFG-TWIG	C
(0021)	WG = WG+5.8E-8*DELTA*IJF	C
(0022)	THETA = THETA+DELTA*WG	C
(0023)	IF(THETA.LT.0.634) GO TO 16	C
(0025)	IF(THETA.GT.1.882) GO TO 16	C
(0027)	IF(TNOW.GT.120.0) GO TO 16	C
(0029)	X = (1-COS(THETA))*0.5	C
(0030)	X1=-0.006825*X+(-3.0) + 0.35*X+(-1.0)	C
(0031)	X2=(1-(0.01365*X+(-1.0) + 0.7*X))+2.0)*0.5	C
(0032)	X3=0.3087*X+(-3.0) + 0.6625*X+(-1.0)	C
(0033)	X4=(1-(-0.6175*X+(-1.0) + 1.325*X))+2.0)*0.5	C
(0034)	NA =10.0-SIN(THETA)*(X1/X2 + X3/X4)	C
(0035)	IF(NA.GT.30.0)	C
(0037)	NN = NA*WG	C
(0038)	QA = NN*YH	C

OL = 34.62E-12. PA

Q R - 0 - 0

$$10 + 10 = 20$$

PSI=HPP/PI

IF (PSI,GE-14.0E6)QR=QA-0.0057*HA*HG

$$QI = QI + QI + QI$$

PSI = HPP/91

$$PA = .93 \cdot PSI$$

VR1TE(6,3)INDV,THETA,V6,9A,PA,HA,IJE,75,IY6,VH,9I,9R

3. FORMAT(E10.4,1X,E10.4,1X,E10.4,1X,E10.4,1X,E10.4,1X,

1E10-4, 1X, E10-4, 1X, E10-4, 1X, E10-4)

CO 10 17

30M11603.91

JOIS

1

8/93/76 8:00 A.M.

XEORIS COMPILER (75/121)

APPENDIX C

ADDITIONAL TESTS OF PROTOTYPE DRIVE

Introduction

The reasons for prototype tests additional to those described in Chapter IV were two-fold: the system "cut-out" several times during normal lock operation, and it was felt that further control adjustments could lower the gate operating time. The cut-outs were due to electrical overload controls associated with the electric motor, the primary cause being additional loads imposed on the gate by water surges in combination with the oversized Pump 1. The KW-charts shown in Figure C1 confirm the deduction.

Since the gate operation is intermittent and of very short duration it was felt that the overload control on the electric motor and its supply could be uprated by 15% without damage to the motor:

- The hydraulic system would in no way be disadvantaged by the power developed.
- To reduce the power overload, and especially the peak power during closure, Figure 4.8(c), system pressure could be reduced somewhat, possibly to 11000 KPa. This would cause the gate operation time to increase from 50 to around 60 seconds.

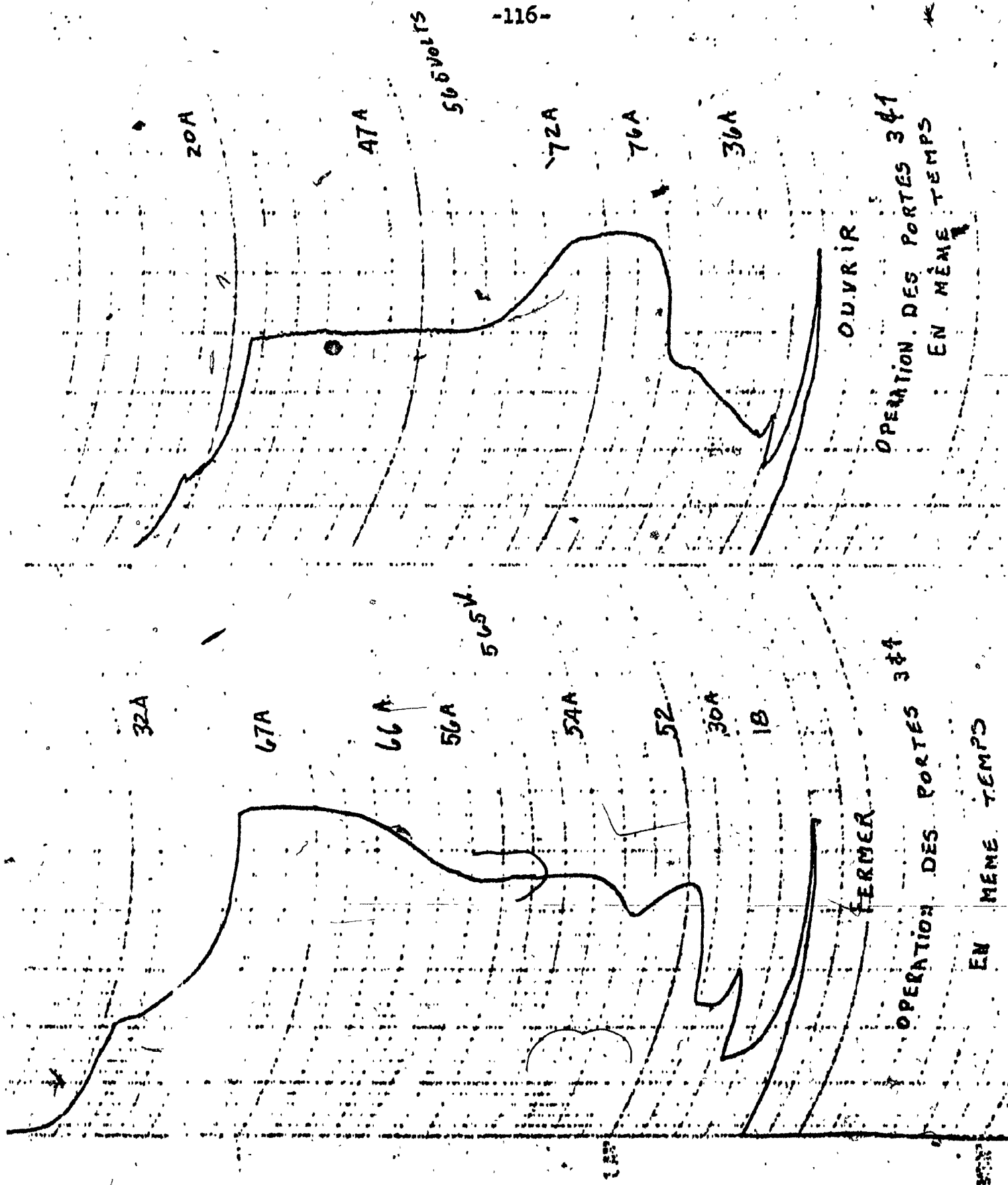


Figure C1 Some Measured Electrical Power Curves

- The disposition of the limit switches dictating Pump 2 cut-in and cut-out could be changed, to improve performance and possibly reduce gate operating time, and the existing overload settings for the electrical motor raised to allow for short term operation above rated power.

It was decided to consider:

- Upgrading the electrical overload controls on system supply,
- drop system pressure somewhat,
- adjusting Pump 2 action limit switches, and tune the system by taking performance measurement traces as the changes are made.

Results

Tests were made to record pressure and motion characteristics as adjustments were made to limit switch strikers controlling gate speed.

Six limit switch actions are required to control pumping for both opening and closing. During gate opening, limit switch action 1 causes Pump 2 cut-in; limit switch action 2 causes Pump 2 cut-out; and limit switch action 3 causes hydraulic set stop when the gate is fully open. During closure, a similar three limit switch action takes place.

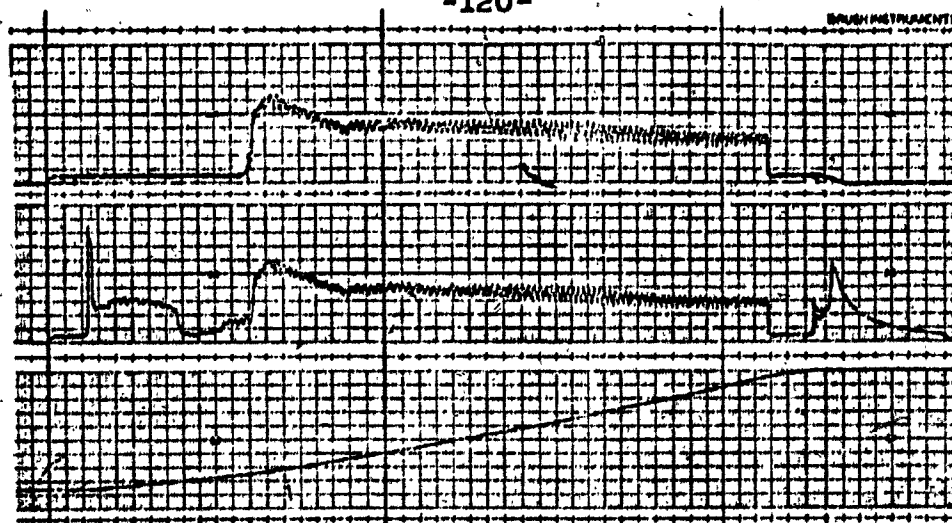
The main area for improvement was to reduce a 10 secs. time delay before Pump 2 cuts in during opening; it was hoped to reduce this to 3 or 4 seconds, enabling Pump 2 to be in action longer and gate operating time to be less. However, only five limit switch units are used, as one unit does dual action. Unfortunately the attempted adjustment was controlled by that limit switch. It meant that any saving by reducing Pump 2 lag during opening was offset by an undesirable shortening of Pump 2 cut-out during closure. If Pump 2 was allowed to run closer to the gate shut point, the gate banged on the lock sill - an undesirable condition. Thus, only minor adjustments could be made and little significant improvement of performance was achieved. However, the tests showed that the drive was operating near its optimum state, with all limitations considered. For future drives, a more precise pump output control appears to be a desirable feature.

Table C1 gives details of the measured results, before and after adjustment. Figure C2 shows recorded pressure and motion traces for the gate opening state. Figure C3 shows the characteristics for gate closing.

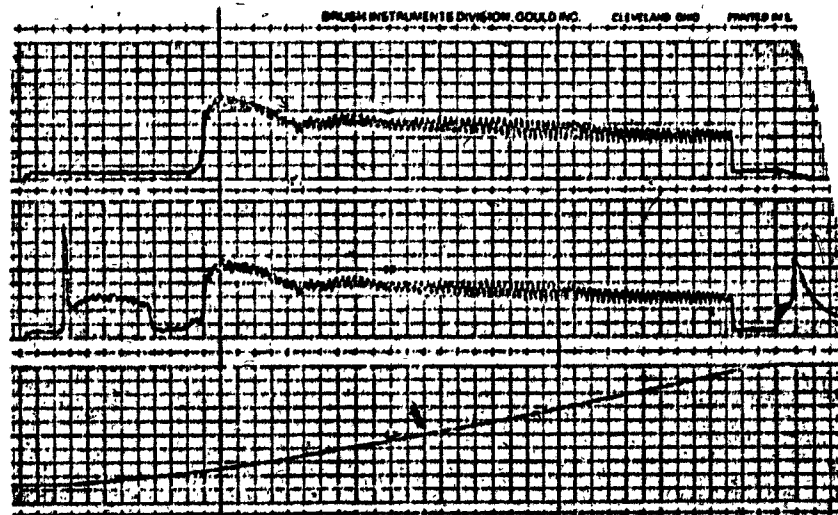
A revealing comparison can be made of Figure C2(a) or (b) against Figure C2(c) and Figure C3(a) or (b) against Figure C3(c).

Run Description	Gate Motion Time Seconds	Pump 2 Time Seconds	Cut-in Time Delay, Pump 2, Seconds	Cut-out Lead, Pump 2, Seconds	Max ^m Pressure KPa	Max ^m Drive Speed rpm	Max ^m Pump Power HP
<u>Gate Opening Runs:</u>							
29 April, both gates	50	36	10	4	13300 for 6 sec	8	
9 June, single gate, before adjustment	43	31.5	9.5	3	11200 for 2 sec	8	
9 June, single gate, after final adjustment	42.5	32	8	3	10500 for 2 sec	8	
9 June, both gates, final run	50	38.5	8	3.5	13300 for 9 sec	8	
<u>Gate Closing Runs:</u>							
29 April, both gates	50	36	4	10	13300 for 6 sec	8	85
9 June, single gate, before adjustment	42	32	3	7	9800 for 2 sec	8	
9 June, single gate, after final adjustment	43	36	2.5	4.5	9800 for 2 sec	8	
9 June, both gates, final run	50	39.5	2.5	8	13300 for 4 sec	8	

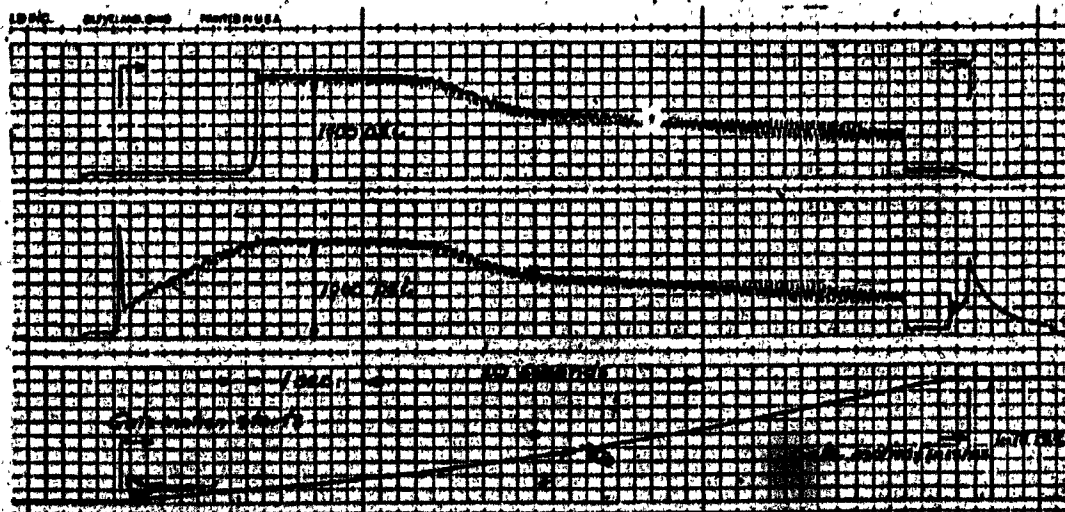
Table C1 Synopsis of Test Runs, with Previous Test Means Included



a. Single Gate Opening, Before Adjustment



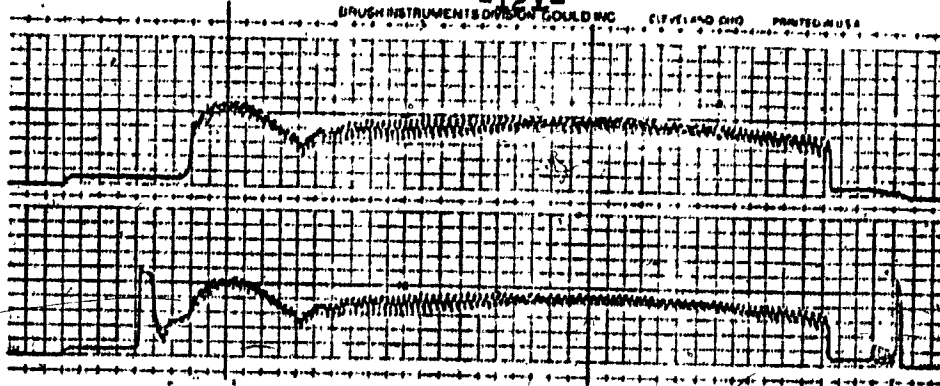
b. Single Gate Opening, After Final Adjustment.



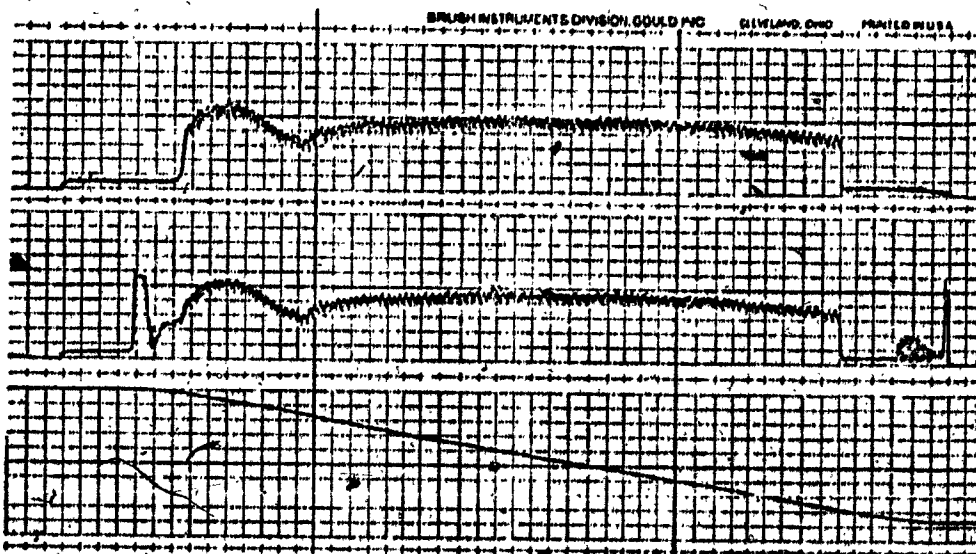
c. Both Gates Opening After Final Adjustment

FIGURE C2

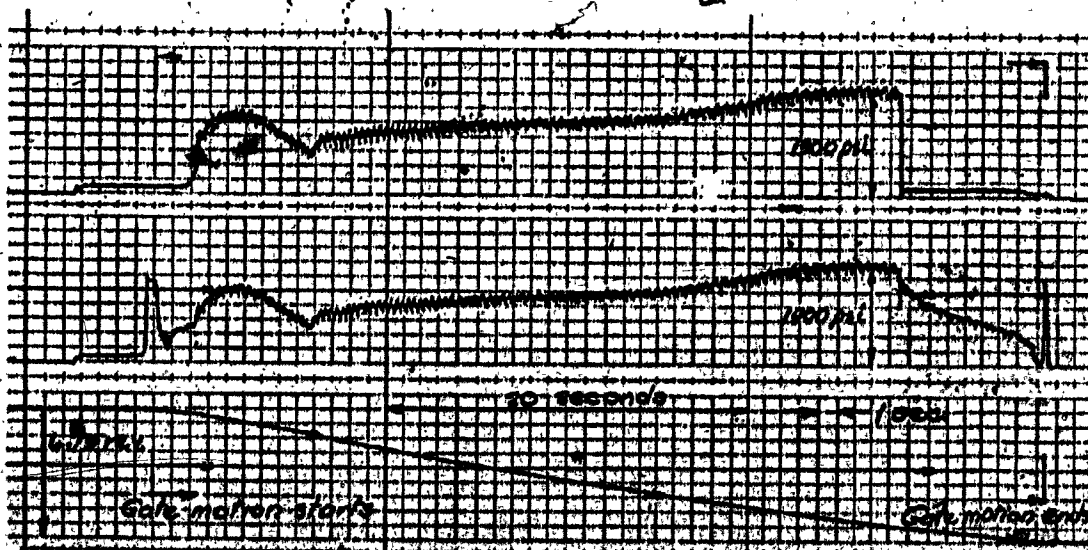
GATE OPENING CHARACTERISTICS



a. Single Gate Closing, After Initial Adjustment.



b. Single Gate Closing, After Final Adjustment.



c. Both Gates Closing, After Final Adjustment.

FIGURE C3

GATE CLOSING CHARACTERISTICS

It is much easier and faster to move a single gate. However, desinchronizing gate operation has been tried and proven not to save operating time during a complete cycle of a pair of gates [11].

For gate opening, Pump 2 stays in at least two seconds longer than previously. However, the gate motion time (50 seconds) is the same as before the adjustment. The pressure traces show that the relief valve remains open longer (9 seconds instead of 6), dumping more flow than previously, and not permitting the small potential speed increase to be realized. Maximum drive shaft speed was 8 R.P.M. just before Pump 2 cuts out. Maximum hydraulic power occurs for the period following Pump 2 cut-in. The power-time characteristic is similar to Figure 4.7(c). Pump 1 operating alone induces drive shaft speed of 3.5 R.P.M. confirming the previous measurements and assessments.

For gate closure, there are also small changes in Pump 2 operation times, without significant change in overall gate motion time (50 seconds before and after adjustment). However, the drive shaft speed just before Pump 2 cut-out is reduced from 6 to 5.5 R.P.M. This is the point on Figure 4.8(c) where system peak power (87 HP) occurred. The peak power indicated on Figure 03(c) is 75 HP, a highly desirable decrease.

Conclusion

The tests were concerned with primary performances of the hydraulic drive - the pressure levels in the working system and the motion of the drive. Factors which emerged, and which could help in the development of future designs included:

- The desirability of improving the control of the various pump actions, in order to allow optimum tuning of the drive;
- the need to improve the power-time characteristic during gate motion, and the correlation of this with primary drive (electric motor and its controls) characteristics;
- possible simplifications of future hydro-mechanical drives in the light of increased availability of performance data, and experience.
- the need to reduce noise in the working system which appeared somewhat excessive (no measurements taken).

Generally, during the tests and subsequent operation in service, the system has proven itself to be highly reliable, requiring no breakdown maintenance.

APPENDIX D

PROPOSED CONTROL CIRCUIT FOR HYDRO-MECHANICAL GATE DRIVES

General

The prototype tests described in Appendix C have shown the negative effect certain controls have on operating times of gate drives. The constant power drive at the optimum power of 25 HP is self-governing and produces an acceptable gate impact speed at the termination of a cycle. Precautions have to be taken to ensure that normal speeds are not exceeded at the end of a cycle. The proposed controls are designed to do this.

Proposed Controls

The controls would take advantage of the possibility of controlling the flow output of the constant power pump by limiting its swash angle to correspond to the maximum output desired at a given gate pivoting position. On a pump of the type employed on the prototype this can be done by preventing a lever connected to the swash plate from exceeding a certain angle. The method proposed for blocking the swash is by the use of two binary cylinders approximating the required lever blocking position by four steps. The cylinder could be controlled by fluidic logic as described schematically in Figure D1.

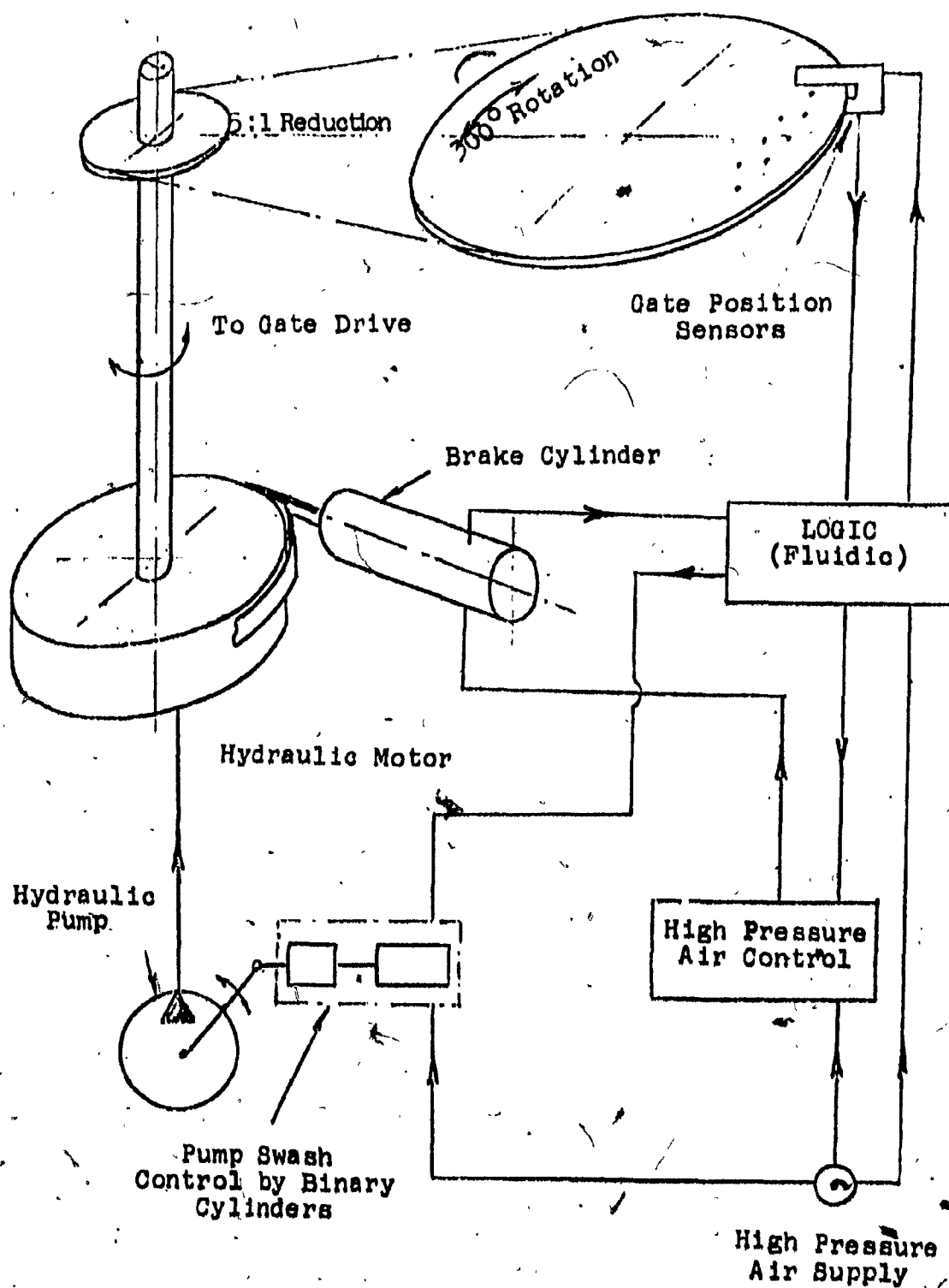


Figure D1 Schematic of Control Circuit

The detailed control circuit is shown in Figure D2. The circuit would also combine the function of applying a band brake to the hydraulic motor when the gate is stationary, and provide the start-stop and emergency shut-down functions.

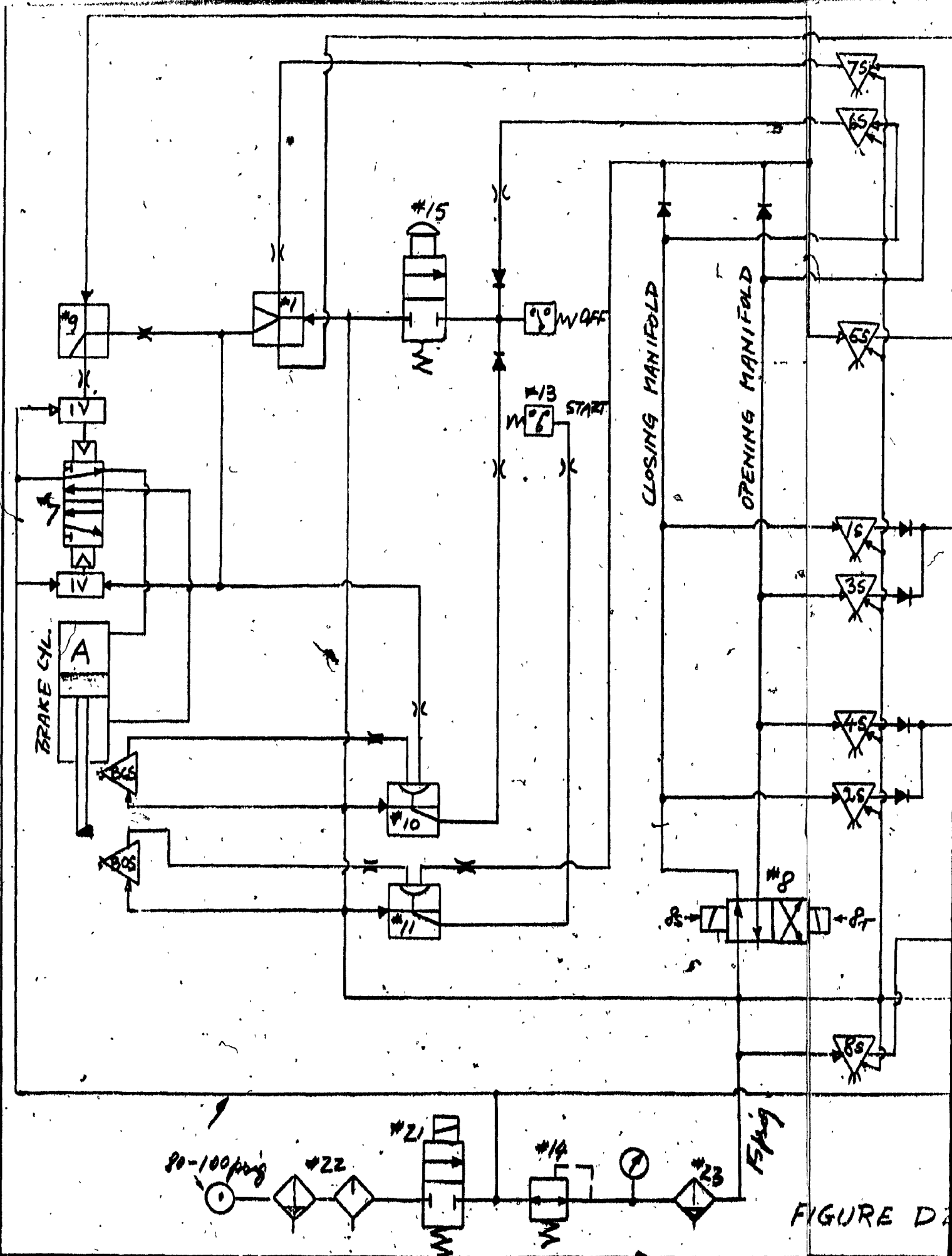


FIGURE D

